

Review

Not peer-reviewed version

---

# Altermagnetism and Altermagnets: A Brief Review

---

[R. Tamang](#) , Shivraj Gurung , [D. P. Rai](#) <sup>\*</sup> , [Samy Brahimi](#) , [Samir Lounis](#)

Posted Date: 21 May 2025

doi: 10.20944/preprints202505.1649.v1

Keywords: altermagnets; non-relativistic Spin-splitting; broken time-reversal symmetry; crystal symmetry





Preprints.org is a free multidisciplinary platform providing preprint service that is dedicated to making early versions of research outputs permanently available and citable. Preprints posted at Preprints.org appear in Web of Science, Crossref, Google Scholar, Scilit, Europe PMC.

Copyright: This open access article is published under a Creative Commons CC BY 4.0 license, which permit the free download, distribution, and reuse, provided that the author and preprint are cited in any reuse.

Disclaimer/Publisher's Note: The statements, opinions, and data contained in all publications are solely those of the individual author(s) and contributor(s) and not of MDPI and/or the editor(s). MDPI and/or the editor(s) disclaim responsibility for any injury to people or property resulting from any ideas, methods, instructions, or products referred to in the content.

## Article

# Altermagnetism and Altermagnets: A Brief Review

R. Tamang <sup>1,2</sup>, Shivraj Gurung <sup>2</sup>, D. P. Rai <sup>1,3,\*</sup> , Samy Brahimi <sup>3,4</sup>, Samir Lounis <sup>3,5</sup> 

<sup>1</sup> Department of Physics, Mizoram University, Aizawl-796004, India

<sup>2</sup> Physical Sciences Research Center (PSRC), Department of Physics, Pachhunga University College, Aizawl-796001, India

<sup>3</sup> Peter Grünberg Institute, Forschungszentrum Jülich and JARA, Jülich, Germany; s.lounis@fz-juelich.de

<sup>4</sup> Laboratoire de Physique et Chimie Quantique, Université Mouloud Mammeri de Tizi-Ouzou, 15000 Tizi-Ouzou, Algeria

<sup>5</sup> Faculty of Physics, University of Duisburg-Essen and CENIDE, Duisburg, Germany

\* Correspondence: dibyaprakashrai@gmail.com

**Abstract:** Recently, a new magnetic phase, termed altermagnetism, has caught the attention of the magnetism and spintronics community. This magnetic phenomenon differs from traditional ferromagnetism and antiferromagnetism. It generally lacks net magnetization and is characterized by unusual non-relativistic spin-splitting and broken time-reversal symmetry. This leads to novel transport properties, such as the anomalous Hall effect, the crystal Nernst effect, and spin-dependent phenomena. Spin-dependent phenomena such as spin currents, spin-splitter torques, and high-frequency dynamics emerge as key characteristics in altermagnets. This paper reviews the main aspects pertaining to altermagnets by providing an overview of theoretical investigations and experimental realizations. We discuss the most recent developments in altermagnetism and prospects for exploiting its unique properties in next-generation devices.

**Keywords:** altermagnets; non-relativistic spin-splitting; broken time-reversal symmetry; crystal symmetry

## 1. Introduction

During the past few decades, there has been a notable shift in focus from traditional ferromagnetic spintronics to antiferromagnetic systems, driven by the increasing demand for energy-efficient and scalable devices [1–3]. The ferromagnets (FMs) are often associated with stray fields, which can cause device malfunction [1]. To overcome this challenge, the robustness of the antiferromagnets (AFMs) against external perturbation appears promising in the realm of spintronics. However, AFMs exhibit degenerate bands in momentum space, and time-reversal symmetry (TRS) combined with translation or inversion is also preserved in AFMs; hence, they lack spin-polarized currents. In this context, altermagnets (AMs) emerge as a magnetic phase that leverages the advantages of both conventional magnetic phases (FMs and AFMs) [4–6].

Altermagnetism is associated with the breaking of TRS and the lifting of Kramers' degeneracy, characterized by the symmetries of spin and real space (discussed in Section 2), without requiring relativistic spin-orbit coupling (SOC). This leads to a nonrelativistic spin splitting (NRSS) of the band structure. The two main phases of magnetism have previously been understood as follows: antiferromagnetism, in which spin alignment is antiparallel and cancels out net magnetization, and ferromagnetism characterized by parallel spin alignment producing net magnetization [7] (see Figure 1a). The model band structures of FM, AFM, and AM are compared in Figure 1b, illustrating the distinct nature of AMs, where spin splitting alternates in momentum space even without the presence of SOC and can reach large magnitudes.

Notably, altermagnets are characterized by spin symmetries giving rise to spin densities with  $d/g/i$ -wave parity (shown in Figure 2) [4,5], which can be regarded as the magnetic counterparts of unconventional superconductors [5] and as realizations of nematic states in both real and spin spaces.

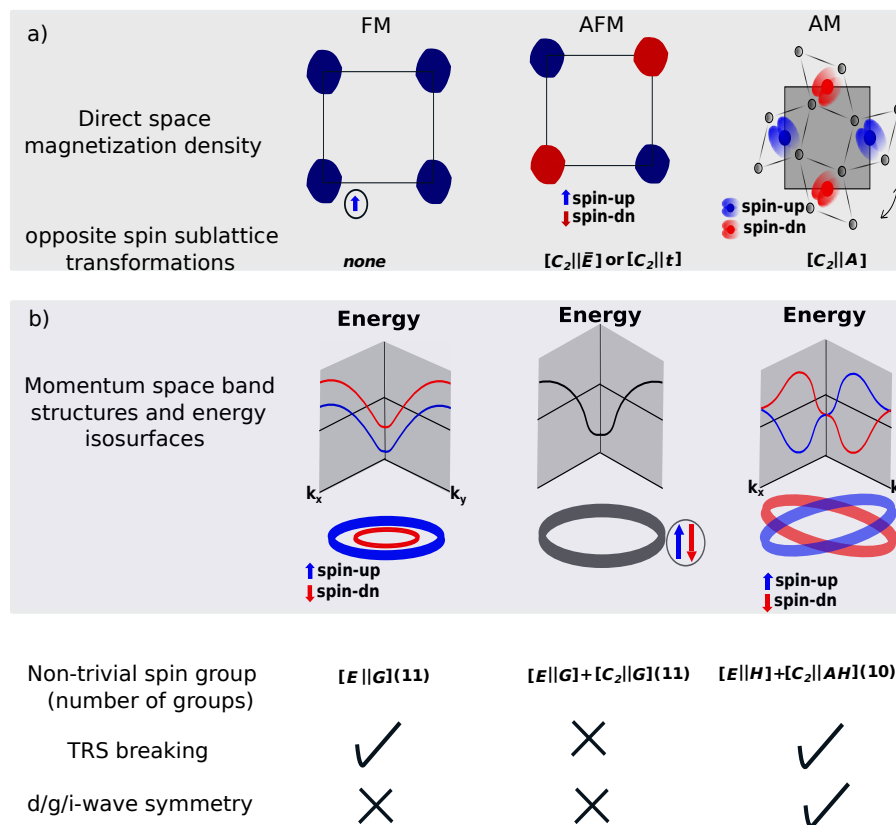


**Figure 1.** a) Ferromagnetic phase, compared to an antiferromagnetic phase with compensated magnetic ordering. Altermagnetic  $\text{RuO}_2$  with d-wave symmetry of the magnetic Ru (red and blue) atoms and the non-magnetic O (grey) atoms, the double-headed arrow indicates that two opposite spin sub-lattices are connected by rotation only. b) Comparison of the momentum space schematic Band structures of ferromagnetic, antiferromagnetic, and altermagnetic phases followed the iso-surface depicted at the bottom of the diagram. FMs show constant spin-splitting in the momentum space, whereas AFMs show no spin-splitting. However, the Band structure corresponding to AMs shows significant alternating spin-splitting. These figures are reproduced from Ref. [4,5] under CC BY 4.0 International license. Published by APS, copyright 2022.

Historically, spin splitting in non-centrosymmetric, high-Z compounds was attributed to SOC, as demonstrated in the seminal works of Rashba and Dresselhaus [8,9]. However, these materials often suffer from chemical instability [10], necessitating alternative pathways for achieving spin splitting in centrosymmetric, thermodynamically stable, low-Z antiferromagnets. One such example is  $\text{MnF}_2$ , a rutile-structured AFM material, where conventional SOC-driven mechanisms cannot account for the observed spin splitting [10].

Altermagnetism arises from electron-electron interactions and the influence of crystal lattice potentials on single-particle states [11]. The local atomic environment, particularly the bonding between magnetic and non-magnetic atoms, plays a crucial role in shaping spin-splitting properties in AMs [12]. The systematic distortion of the local environment from a hypothetical high-symmetry phase can lead to distorted phases depending on the second-rank symmetric tensor  $\hat{U}$ 's, potentially resulting in altermagnetism when the magnetization is compensated [12] as illustrated in Figure 3. The underlying mechanism may be linked to the spin-polarized even-parity wave Pomeranchuk instability—a purely electronic instability of the correlated Fermi liquid that distorts the Fermi surface [13,14].

While altermagnets are discussed in their collinear phase [6], they can also arise in non-collinear orders as comprehensively discussed in Ref. [15]. In fact, a wide range of materials, including metals, semiconductors, insulators, and superconductors, can intrinsically exhibit altermagnetism [4]. Additionally, material design concepts can be used to induce it, as discussed in Section 4.3.

To identify AMs, Smejkal *et al.* [4] proposed the following theoretical criteria:

- The number of magnetic atoms in a unit cell is even.
- The magnetic atoms in AMs are not related by inversion symmetry.
- Non-interconvertible local motif-pair spin anisotropy.
- The opposite-spin sublattices are connected by rotation (in spin and real spaces) or combined with translation or inversion symmetry, mirror, glide, or screw.

Such an identification is automated and can be readily found using a computational tool developed by Smolyanyuk *et al.* [16] using a Crystallographic Information File as input.

First-principles computations demonstrated NRSS in various materials, with more than 200 compounds in bulk and 2D predicted as candidate AMs [17]. Using a machine learning-based approach, potential candidates have been identified based on their electronic structures [18]. However, only a limited number have been experimentally investigated (as shown in Table 1), resulting in the discovery of only a few material candidates. Indeed, advanced experimental methods such as neutron scattering, magnetic resonance, and advanced spectroscopic techniques can probe the unique spin structures of AMs. This paves the way for exploring a wide range of two-dimensional (2D) and bulk materials that could potentially host this novel magnetic phase.

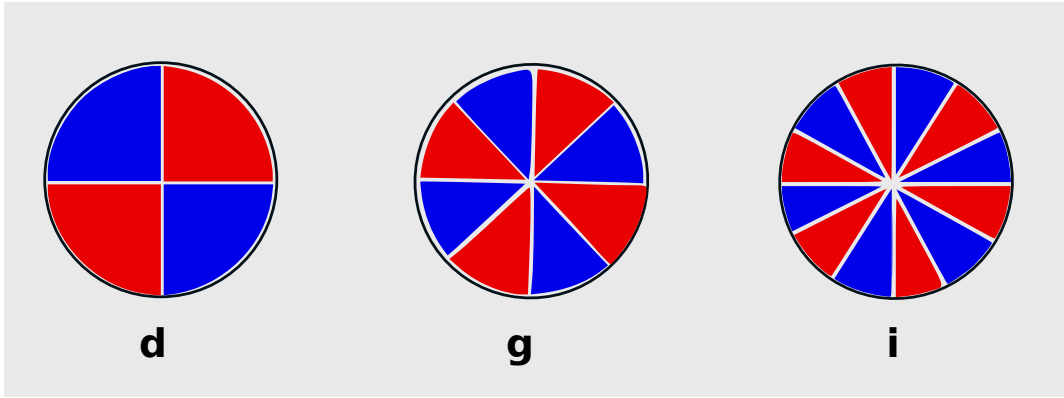


**Figure 2.** Schematic d-, g- and i- even-parity waveform of AMs depicted in 2D. The figure is adapted from ref [5] under CC-BY 4.0 International license. Published by American Physical Society(APS).

Beyond fundamental interest, AMs hold immense potential for spintronic applications due to the emergence of spin-currents [19–22], spin-splitter torques [23,24], efficient spin-to-charge conversion [25,26], and giant/tunnel magnetoresistance [27–32] effects, exotic phenomena linked to superconductivity [33–57], high-frequency dynamics (THz) [58,59], and distinct topological states [34,60–62]. In general, these properties promote AMs as promising materials for information technology [58,63]. Spintronic devices would switch faster and operate at lower power compared to conventional charge-based electronics [64,65].

**Table 1.** NRSS on various altermagnetic materials from multiple forms of ARPES experiments.

Materials	Space Group	NRSS detection	Reference
CrSb	$P6_3/mmc$	✓	[81,88–90]
MnTe	"	"	[72,94,96]
MnTe <sub>2</sub>	$Pa\bar{3}$	"	[97]
KV <sub>2</sub> Se <sub>2</sub> O	$P4/mmm$	"	[100]
Rb <sub>1-δ</sub> V <sub>2</sub> Te <sub>2</sub> O	$P4/mmm$	"	[99]
GdAlSi	$I4_1/md$	"	[113]
RuO <sub>2</sub>	$P4_2/mnm$	"	[98,114]
CoNb <sub>4</sub> Se <sub>8</sub>	$P6_3/mmc$	"	[115,116]
Co <sub>1/4</sub> NbSe <sub>2</sub>	$P6_3/mmc$	"	[117,118]
RuO <sub>2</sub>	$P4_2/mnm$	×	[95]



While theoretical studies have advanced rapidly in the field of AMs, experimental verification and material realization remain in their early stages. This review aims to provide a concise overview of recent developments, clarify fundamental concepts, and highlight potential applications, along with methods for inducing altermagnetism. We begin by discussing the spin group theory used to understand the formation of altermagnets from a symmetry perspective. Next, we review the experimental and theoretical techniques employed to explore the emergence of altermagnets, followed by an examination of the materials studied in this context. We then discuss magnetotransport phenomena and promising applications before concluding with key insights.

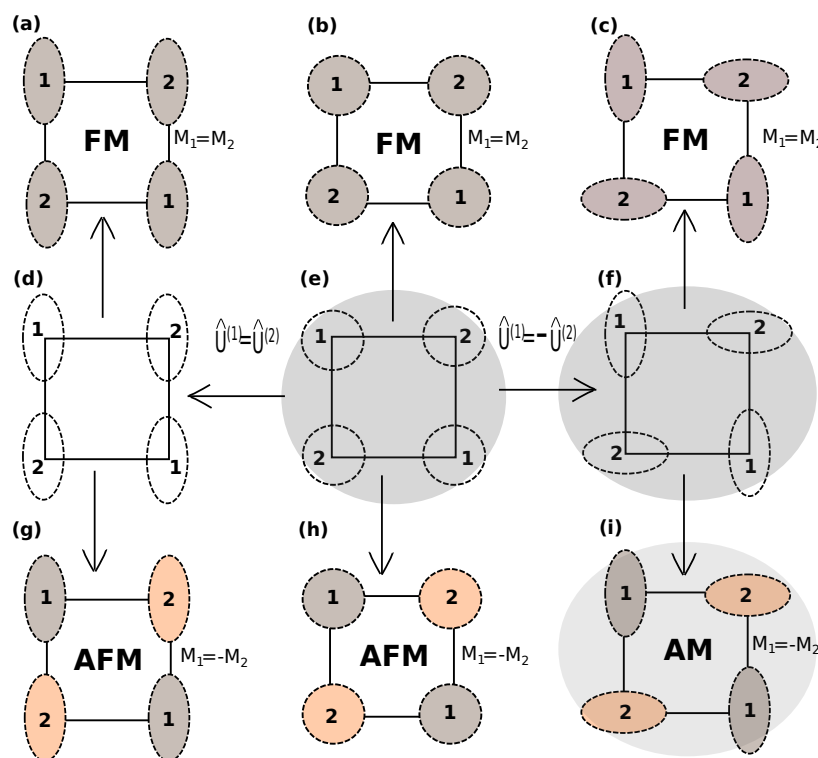


**Figure 3.** (a to c) represent the ferromagnetic phases (FM with  $M_1 = M_2$ ) while (g to i) represent the staggered magnetic phases (AFM or AM with  $M_1 = -M_2$ ) and (d, f) are structural phases. Any magnetic phase can be derived from the highly symmetric hypothetical phase demarcated in (e) with no magnetic order and an isotropic local environment of magnetic atoms (shown with circles). The distortion of local environment leads to two different structural phases with equal ( $\hat{U}^{(1)} = \hat{U}^{(2)}$ ) or distorted ( $\hat{U}^{(1)} = -\hat{U}^{(2)}$ ) local environment ( $\hat{U}$ 's are second rank symmetric tensor illustrating feasible distortion of the sublattices). Combining the staggered environment with the staggered order gives altermagnetism. The sign of the exchange coupling between atoms 1 and 2 determines whether the magnetic order results in staggered ( $M_1 = -M_2$ ) or ferromagnetic ( $M_1 = M_2$ ) structures. This figure is reproduced from Ref. [12] under CC-BY 4.0 International License. Published by Springer Nature, copyright 2024.

## 2. Spin Group Theory Description

Landau theory is traditionally used for ferromagnets and antiferromagnets. The theoretical foundation laid by identifying a set of multipolar secondary order parameters bridges the gap between ideas about spin symmetries and the observable properties of these materials. McClarty *et al.* combined the Landau theory framework, emphasizing the importance of incorporating spin-space symmetry into the analysis [66]. The thorough theoretical approach describes AM's behavior in a range of scenarios. Recently, the approach used by Smejkal *et al.* [4,5] to explain NRSS magnetic materials uses a description of magnetic group theory, where spin and space symmetries are decomposed. The transformation used as such  $[C_i || C_j]$ , the transformation left side of the double vertical line acts in

the spin space, and the transformation right side of the double vertical line acts in real space. In case of RuO<sub>2</sub> the related spin group symmetry is  $[C_2||C_{4z}t]$  [4]. Here, twofold( $C_2$ ) rotation in spin space and fourfold rotation( $C_{4z}$ ) are merged with the translation (t) in the real space. If  $r_s$  corresponds to a spin-only group containing the transformation solely in the spin space, and  $R_s$  is the nontrivial spin group containing the transformation like  $[C_i||C_j]$ , however not containing elements of the explicit spin-only group, then the spin group can be expressed as the direct product  $r_s \times R_s$  [67,68]. The explicit spin-only group is defined by  $r_s = C_\infty + \bar{C}_2 C_\infty$ , here  $C_\infty$  is the group containing all the spin space rotational transformations about the spins' common axis, and  $\bar{C}_2$  is the two-fold rotation about an axis orthogonal to the spin, followed by reversal of spin space. Consequently, the symmetry operation  $C_\infty$  makes spin a good quantum number. Hence, the band structure is accompanied by the split-band structure of the spin-up and spin-down channels. The three types of nontrivial spin Laue groups can describe different types of magnetic materials. The foremost kind is for ferromagnetic materials, where the group is represented by  $R_s^I = [E||G]$ , where G specifies the Laue group.  $R_s^I$  defines the non-trivial spin group corresponding to conventional ferromagnetism (spin-split band structure with broken TRS symmetry). The second type of non-trivial spin group is  $R_s^{II} = [E||G] + [C_2||G]$ . The group  $R_s^{II}$  also describes conventional antiferromagnetism and the related opposite spin sublattice symmetry is  $[C_2||\bar{E}]$  or  $[C_2||t]$ , where  $\bar{E}$  is the real space inversion and t denotes translation.

$R_s^{III} = [E||H] + [C_2||AH]$  gives the nontrivial spin group that characterizes the AMs.  $H$  is the Halving subgroup possessing half elements of the real space transformation of the nonmagnetic Laue group  $G$ , which includes the identity element of real space, and  $E$  stands for the spin space identity transformation. The  $G - H = AH$  contains the residual half of the transformation, where  $A$  is the real space rotation (proper or improper, symmorphic or non-symmorphic). Only real space transformations that exchange atoms between sublattices of the same spin are contained in  $H$ , and exclusive real space transformations that exchange atoms between sublattices of opposite spin are present in  $G - H$ . The non-trivial spin subgroup  $[E||H]$  allows the symmetry in such a manner that spin sublattices are characterized by anisotropic spin densities. Similarly,  $[C_2||AH]$  is responsible for broken TRS and non-relativistic spin splitting of bands. Together, there are ten nontrivial spin Laue groups categorizing d-, g-, and i-wave AMs [4,5].

### 3. Experimental Techniques and Theoretical Approaches to Explore Altermagnetism

The field of altermagnetism has been driven by theoretical predictions. There is currently a large database of materials predicted to host an altermagnetic behavior. Here, we review the techniques used experimentally and theoretically to address altermagnetism (see for example, Table 1).

Various experimental methods have been employed to confirm NRSS in AMs, with angle-resolved photoemission spectroscopy (ARPES) being a key technique. ARPES operates on the principle of the photoelectric effect [69,70], where a spectrometer records the intensity  $I$  of emitted photoelectrons based on their kinetic energy  $E_k$  and emission angle  $\alpha + \beta$ . A schematic of the experimental ARPES basic setup is shown in Figure 4. This technique directly maps a material's energy-momentum (E-k) relationship [71]. The pioneering work of Lee *et al.* marked the first application of ARPES in AMs, using epitaxial thin films of MnTe synthesized in situ to conduct temperature-dependent ARPES studies. Their findings revealed the lifting of Kramer's degeneracy and confirmed that above the Néel temperature, NRSS vanishes, signifying a magnetic phase transition [72].

Over the past few decades, ARPES has undergone remarkable advancements, both in technology and scientific applications. The development of advanced light sources, particularly third-generation synchrotrons [73–78], has significantly enhanced its capabilities. Additionally, extending ARPES into the soft and hard X-ray range [73,77,79,80] has broadened its application spectrum. More recently, Ding *et al.* [81] utilized synchrotron-based high-resolution ARPES to successfully detect NRSS in CrSb, highlighting the technique's growing sophistication and increasing relevance in uncovering novel electronic properties.

The ARPES signal is strongly influenced by photon energy and polarisation, as dipole matrix elements shape the photoemission process [82]. Soft X-ray ARPES (SX-ARPES), with its deeper probing capabilities, is particularly advantageous for studying buried interfaces and capped surfaces [71]. By resonantly probing valence d- and f-states, it provides crucial insights into strongly correlated systems, including Mott insulators, superconductors, and magnetic materials [83,84]. Additionally, the use of high photon energies in SX-ARPES enhances penetration through complex surface structures, reducing the impact of relativistic spin splitting [85]. This technique has also been instrumental in investigating oxide-based heterostructures [86] and superlattices [87], further expanding our understanding of quantum materials. Recent studies have employed angle-dependent SX-ARPES to examine the altermagnetic characteristics of thin epitaxial CrSb films [81,88–90]. The measurements reveal a significant spin splitting of approximately 0.6 eV below the Fermi level [88] (see Figure 4c), aligning well with theoretical predictions for AMs [4]. Moreover, CrSb exhibits a high Néel temperature of 703 K, making it a promising candidate for room-temperature applications [90].

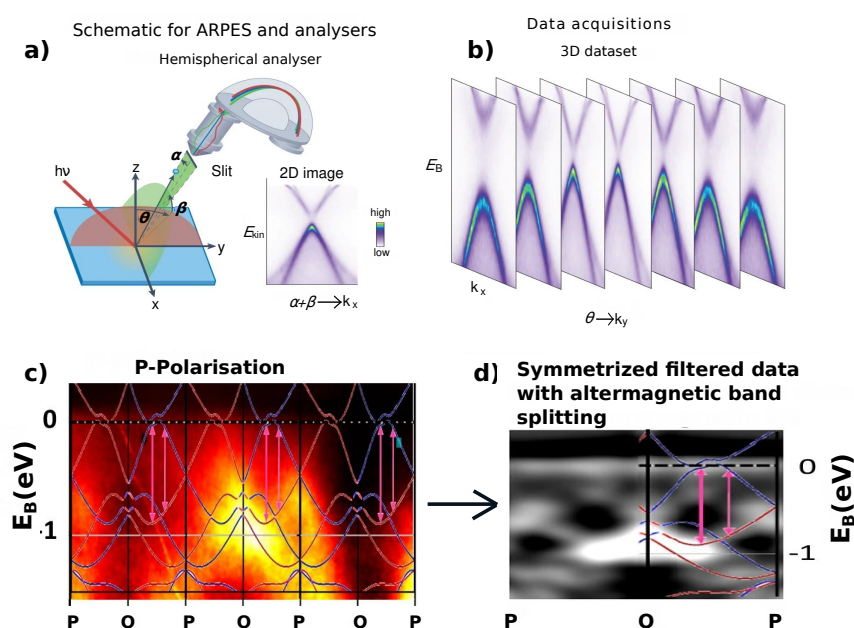


**Figure 4.** a) Schematic ARPES experimental setup b) ARPES mapped band structure at different sample  $\theta$  values. Figures a) and b) are reproduced with permission [71]. Copyright 2022, Springer Nature. (c,d) The spin-integrated SX-ARPES intensity just below the Fermi energy, showing distinct spin splitting: c) High symmetry P-Q path with p-polarized photons. d) Symmetrized filtered data using the Laplacian filter. Figures c) and d) are reproduced from Ref. [88] under CC BY 4.0 International license. Copyright 2024, published by Springer Nature.

Another significant advancement is spin-resolved ARPES (Spin-ARPES), which extends the technique by resolving the spin vector direction of electrons with high energy and momentum precision [91–93]. However, its efficiency is lower, leading to longer data acquisition times [71]. Despite this limitation, various forms of ARPES have been successfully employed in multiple AMs to detect NRSS, further reinforcing its importance in the study of novel magnetic materials [72,81,88–90,94,94–100].

Although ARPES provides direct evidence of NRSS, measuring spin splitting using ARPES is challenging. Foremost, spin polarization in the measured band structure can cancel out due to contributions from mixed domains, as separating altermagnetic domains is often difficult [72]. For example, the Helium discharge lamp with mm-scale beam spot is much larger than individual magnetic domains, and the signals from multiple domains blend together, canceling out any net polarization [72]. To address this issue, spin-resolved micro- or nano-ARPES, with a micro- or nanometer-scale beam spot, can be a desirable approach for determining NRSS [71,96].

Besides ARPES, various experimental techniques and theoretical frameworks have been used to investigate AMs, as summarized below.

- High field torque magnetometry applied on FeSb<sub>2</sub> to map the Fermi surface. [101].
- Neutron scattering and Muon spin rotation/relaxation ( $\mu$ SR) techniques: used for RuO<sub>2</sub> [102],  $\alpha$ -MnTe [103].
- XMCD: X-ray magnetic circular dichroism on MnF<sub>2</sub>, RuO<sub>2</sub> [104,105] and MnTe [106,107].
- DFT (Density Functional Theory): First-principles investigations can be efficiently performed at a low computational cost without including SOC on altermagnets. First-principles calculations were performed to provide theoretical predictions to motivate and compare with experimental findings, focusing on various materials including RuO<sub>2</sub> [98,108,109], CrSb [81,88], MnTe [72,94,96], MnF<sub>2</sub> [110,111], and others [112].

## 4. Examples of Explored Altermagnetic Materials

### 4.1. MnF<sub>2</sub> and Octupole Moments

In MnF<sub>2</sub>, the fluorine atoms around the manganese atom at the structure's center are rotated 90° around the z-axis compared to those surrounding the manganese atom at the structure's corner, leading to nonequivalent manganese sites, although the presence of nonequivalent Mn sites raises questions about the exact symmetry classification. The computational study by Bhowal *et al.* [110] explored the role of magnetic octupoles, identifying their potential for tuning via alterations to the fluorine environment around the Mn sites without affecting the spin configuration. This tuning capability demonstrates that flipping the Mn spin arrangements reverses the sign of the octupole moment, highlighting magnetic octupoles as a natural-order parameter for NRSS antiferromagnetism. Magnetic Compton profile measurements were proposed as a tool to detect associated magnetic octupoles [110]. These findings suggest promising research directions, particularly the investigation of other magnetic materials with a centrosymmetric tetragonal rutile structure. The potential role of magnetic octupoles as order parameters in these systems warrants further detailed exploration.

### 4.2. Contradicting Reports on the Magnetic Ordering of RuO<sub>2</sub>

Although RuO<sub>2</sub> stands out as the most explored material for altermagnetism, its magnetic properties have been the subject of conflicting results, with some suggesting Pauli paramagnetism [119] in the past. In contrast, others indicate an antiferromagnetic configuration [120,121].

Assuming a Hubbard-U of 2 eV [108], the first principles simulations, confirmed experimentally, revealed significant NRSS in RuO<sub>2</sub> [4,98,114]. However, considering a zero U or a realistic value leads to a non-magnetic state, as shown in the detailed study as a function of U for stoichiometric RuO<sub>2</sub> in Ref. [122]. The study was also carried out for non-stoichiometric RuO<sub>2</sub>, proposing that Ru vacancies could facilitate a magnetic state. This hypothesis is supported by the observation that hole-doped RuO<sub>2</sub> modeled by varying the electron counts in the DFT calculations can exhibit magnetic properties. Hence, the occurrence of altermagnetism depends on the sample's stoichiometry, with nonstoichiometric samples showing potential for magnetism due to Ru vacancies or hole doping. More recently, ab initio simulations have predicted that altermagnetism can be stabilized in ultrathin RuO<sub>2</sub> films even without the inclusion of a Hubbard-U term [123]. In these thin films, strong layer relaxations significantly modify the electronic states, effectively mimicking the effects typically induced by a finite U. Such an observation goes in line with recent studies on the impact of strain in thin films on the emergence of altermagnetism [124–127].

The study by Smolyanyuk *et al.* [122] could potentially clarify the significant variability in experimental observations, which may be due to differences in sample conditions, underscoring the need for a more detailed characterization of RuO<sub>2</sub> stoichiometry in future studies. The study of Brahimi *et al.* [123], on the other hand, indicates that the output of the measurements depends on the surface sensitiveness of the experimental techniques.

The magnetic characteristics of RuO<sub>2</sub> were investigated by combining a variety of cutting-edge spectroscopy techniques, including neutron diffraction and muon spin spectroscopy ( $\mu$ SR). It was demonstrated that the magnetic signals previously found are probably the result of experimental errors, such as



multiple scattering at defects rather than intrinsic magnetic features of the material, therefore challenging prior assertions of magnetic order in  $\text{RuO}_2$ . The thoroughness of the methodology ensures high reliability in the results, particularly in ruling out magnetic order in  $\text{RuO}_2$  [102,128]. Furthermore, Liu *et al.* [95] directly analyzed the band structures and spin polarization of single-crystal and thin-film rutile  $\text{RuO}_2$  samples using ARPES and SX-ARPES. The electronic structure of  $\text{RuO}_2$  is reported to be reasonably consistent with non-magnetic conditions, as evidenced by the lack of  $k$ -dependent spin-splitting.

An alternative approach for investigating altermagnetism in  $\text{RuO}_2$  may involve Fermi surface mapping, as demonstrated in recent experimental studies [101]. This method could offer valuable insights into the electronic structure and magnetic characteristics of  $\text{RuO}_2$ , complementing existing spectroscopic and theoretical investigations.

Gomonay *et al.* [12] studied  $\text{RuO}_2$ 's magnon spectra and domain wall dynamics, developing a phenomenological model for altermagnets (AMs). Their framework extends micromagnetic models, revealing lifted magnon degeneracy [129,130], anisotropic spin stiffness, and domain wall properties distinct from antiferromagnets. The model predicts a Ponderomotive force enabling domain wall manipulation via magnetic force microscopy. Additionally, AMs exhibit anisotropic Walker breakdown at high velocities, with sublattice stiffness differences causing domain wall deformations. Based on Landau-Lifshitz equations, the model incorporates anisotropic exchange stiffness to describe altermagnetic behavior. Tunable domain walls hold potential for novel data storage and neuromorphic computing applications [131].

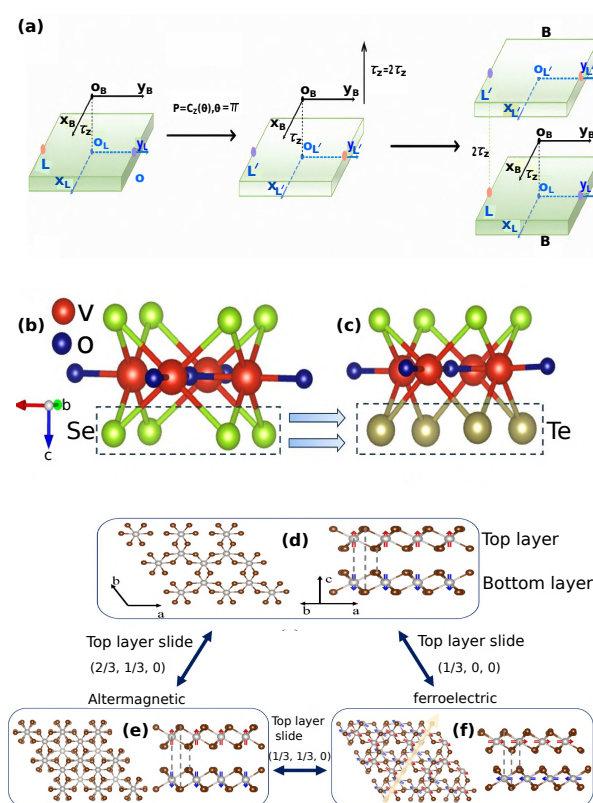


**Figure 5.** Strategies for inducing altermagnetism: Fig a) General stacking of monolayer to form bilayer through a series of rotation and translation operations. The purple and orange solid dots indicate atoms within the unit cell that are altered by the respective symmetry operations. Figure a) is reproduced with permission [132]. Copyright 2022, American Physical Society. b),c) Janus AM  $\text{V}_2\text{SeTeO}$  formed by replacing the bottom Se layer with Te atoms. Figures b),c) are reproduced with permission [133]. Copyright 2023, American Chemical Society. d) Monolayer and bilayer of  $\text{PtBr}_3$ . With suitable sliding of the top layer, either an altermagnetic(e) or ferroelectric(f) phase can be obtained. Figures d)-f) is reproduced with permission [134]. Copyright 2024, American Physical Society.



#### 4.3. 2D AMs and Methods for Designing AMs

Various two-dimensional (2D) materials have been proposed to exhibit altermagnetism [17]. Liu *et al.* [135] identified the 2D altermagnetic semiconductors FeS and FeSe as the thinnest known examples, exhibiting strong magnetic order, low exfoliation energy, and good chemical stability. Both materials feature A-type antiferromagnetic structures with notable spin-splitting magnitudes, 193 meV for FeS and 103 meV for FeSe. Furthermore, magnetic anisotropy energy (MAE) calculations suggest their ability to sustain long-range magnetic order [135].

Monolayer RuF<sub>4</sub> has also been found to exhibit altermagnetism. Inclusion of spin-orbit coupling (SOC) in calculations introduces weak ferromagnetism due to a slight canting of Ru spins [136]. In weak ferromagnets, the Néel vector can be manipulated by a small external magnetic field [137], which offers a potential means of controlling the direction of spin-polarized currents in altermagnets. In addition to the aforementioned, various stacking and twisting techniques can be used to induce AM (shown in Figure 5), particularly in antiferromagnetic bilayers [138]. An effective approach involves Van der Waals (vdW) stacking, where a magnetic vdW monolayer is stacked into a bilayer with the upper layer flipped, introducing an in-plane two-fold rotation. A subsequent twist operation breaks the inversion symmetry, thus inducing altermagnetism [139]. This method applies broadly to magnetic vdW bilayers that exhibit interlayer antiferromagnetic order across all five 2D Bravais lattices. For example, materials such as transition metal oxyhalides [140,141], antiferromagnetic van der Waals materials [142–144], hexagonal lattice MnBi<sub>2</sub>Ti<sub>4</sub> [139].

A notable example is twisted VObR, where a tight-binding model predicts a giant spin Hall angle ( $\Theta=1.4$ ). This tunability, achieved through variations in the twist angle, opens new avenues for efficient spin-current generation [139]. Furthermore, a recent study proposes an altermagnetic Janus monolayer [133,145,146]. Janus V<sub>2</sub>SeTeO, created by substituting the Se atoms in the bottom layer of V<sub>2</sub>Se<sub>2</sub>O with Te atoms, exhibits enhanced piezoelectricity, strain-induced valley polarization, and doping-controlled piezomagnetism, making it a highly promising material for applications in nanoelectronics, spintronics, and valleytronics. First-principles calculations confirm that these properties can be independently tuned via mechanical strain, offering new possibilities for designing multifunctional 2D materials. Stacking followed by sliding demonstrated an effective method for inducing altermagnetism [134].

Moreover, Pan *et al.* [132] proposed a General Stacking Theory (GST) to predict altermagnetism in bilayers based on the symmetry of monolayer components, provided there is antiferromagnetic coupling between the layers. The stacking operator ( $\hat{P}$ ) transforms a monolayer (L) into another layer (L') through a series of symmetry operations, translations, or rotations, forming a bilayer (B) directly [132].

Furthermore, modulating coordination modes enables the tunability of spin-related properties in 2D metal-organic frameworks (MOFs) [147–149]. These materials exhibit high spin-charge conversion ratios, reaching 56.85% for Ca(pyrazine)<sub>2</sub> and 86.04% for Sr(pyrazine)<sub>2</sub>, alongside high spin Hall conductivity. Their ability to control spin currents via electric fields presents exciting opportunities for spintronics applications [148].

These advancements highlight the versatility of 2D altermagnetic materials, demonstrating that approaches such as twisting, stacking, and atomic substitution can effectively engineer spintronic and multifunctional properties across diverse material classes.

The strain has also been identified as a viable method for inducing and modulating altermagnetism by modifying crystal symmetry [124,150,151]. For example, bulk ReO<sub>2</sub> typically adopts an antiferromagnetic monoclinic  $\alpha$  phase but transitions to a tetragonal R phase under pressure, exhibiting altermagnetic behavior [150]. Murnaghan fitting data further suggest that the altermagnetic R-ReO<sub>2</sub> phase is more stable than its monoclinic counterpart. In addition, a recent study suggests that the coexistence of staggered antiferromagnet and orbital order (OO) is capable of producing robust altermagnetism, giving rise to significant spin-splitting and spin-splitter conductivity. Electron correlations can generate a phase in which Neel AFM and staggered OO coexist, producing a d-wave altermagnetic

phase [152]. Various experimental studies have identified staggered orbital ordering on the surface of CeCoIn<sub>5</sub> [153], as well as in transition-metal oxides with a perovskite structure, such as LaMnO<sub>3</sub> [154–156], and in cubic vanadate compounds [157]. The right size of the simulation unit cell plays an important role in predicting the presence of altermagnetism. As demonstrated in the theoretical study by Jaeschke *et al.* [158], enlarging the unit cell of MnSe<sub>2</sub> reveals d-wave altermagnetism, as shown in Figure 6. Several candidates have been identified for d- and g-wave altermagnetism; for example, supercells of perovskites CsCoCl<sub>3</sub>, RbCoBr<sub>3</sub>, and BaMnO<sub>3</sub> exhibit g-wave altermagnetism.

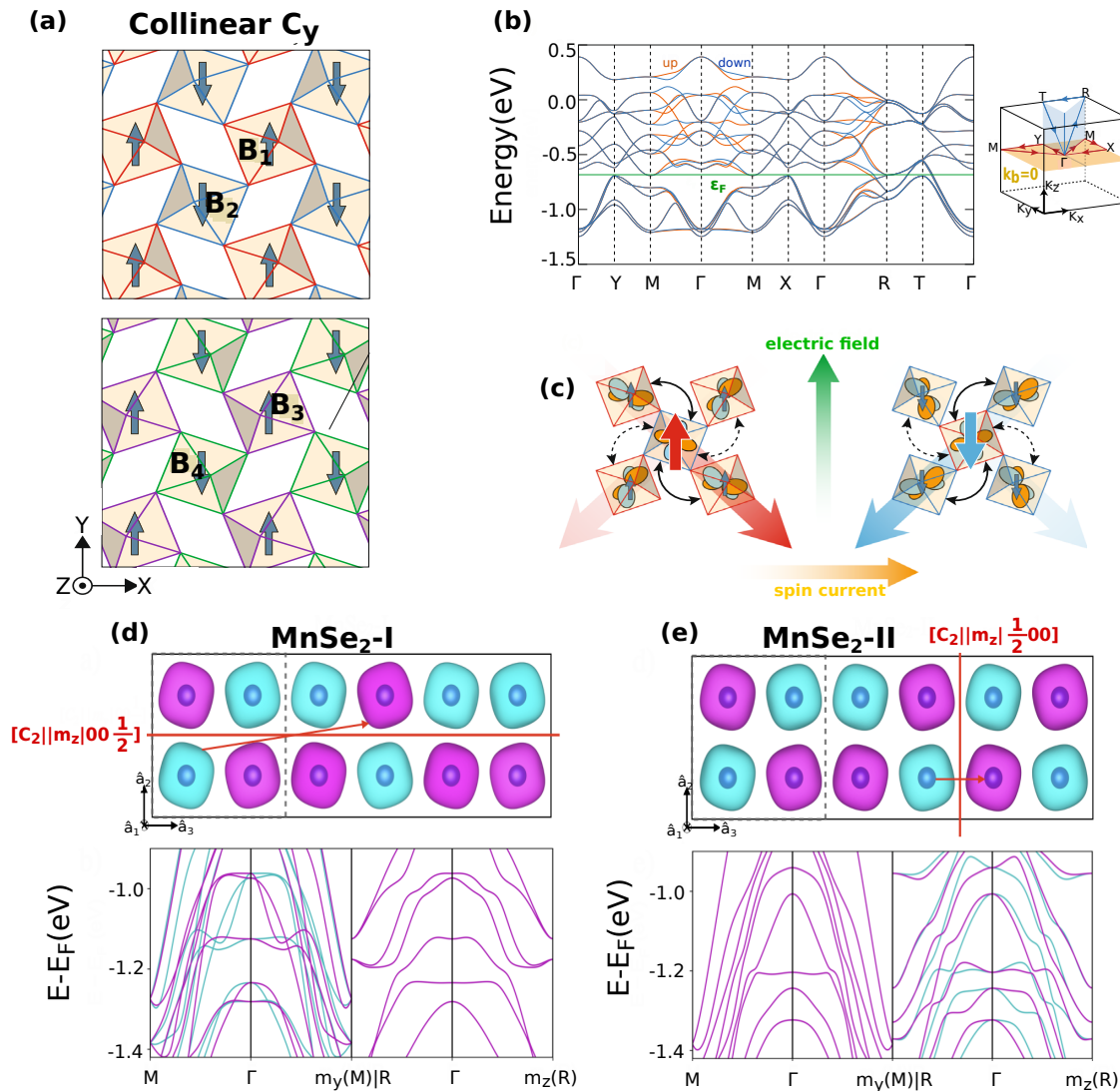


**Figure 6.** Perovskite and supercell altermagnets: a) C-type AFM ordering with GdFeO<sub>3</sub> type lattice distortion parameterized by  $\phi$ . b) Corresponding band structure of  $t_{2g}$  orbital and high symmetry path. c) Schematic representation of spin current generation. d),e) Supercell AMs with opposite spin sublattice connected by glide symmetry and corresponding band structures at the bottom.

#### 4.4. Perovskites

Perovskite is the class of materials having the chemical stoichiometry ABX<sub>3</sub>. They have a diverse range of applications, including photodetectors, solar cells, LEDs, magnetoelectric effects, optoelectronic devices, superconductivity, photovoltaic effects, etc. [159–162]. The combination of antiferromagnetic ordering and GdFeO<sub>3</sub>-type lattice distortions leads to the emergence of altermagnetic properties, the anomalous Hall effect, and spin currents in perovskites [22,163,164]. Ruddlesden-Popper phases and their related perovskite structures also serve as material candidates for altermagnets [163,165]. Perovskites with diverse electron configurations ( $d^n$ ) offer promising candidates for the spin current generation and the anomalous Hall effect (AHE). Among them, CaCrO<sub>3</sub> (3d)<sup>2</sup>, exhibiting C-type

AFM order below 90 K and maintaining metallic conduction, stands out as a potential material [166]. Similarly, C-type AFM order is present in  $\text{AVO}_3$  ( $A = \text{La}-\text{Y}$ ), which can transition to a metallic state through doping of the A-site carrier [167–169]. The spin splitting mechanism may also extend to  $d^4$  systems, such as  $\text{R}_x\text{A}_{1-x}\text{MnO}_3$ , due to  $e_g$ - $e_g$  and  $e_g$ - $t_{2g}$  electron hoppings [170,171]. Furthermore, A- and G-type AFM orders could exhibit spin splitting if metalized through carrier doping or proximity effects [164,172]. Beyond these,  $d^3$  systems, including  $\text{LaCrO}_3$  and  $\text{YCrO}_3$ , display AFM states that potentially support AHE [173–175]. Mn-based perovskites, such as  $\text{CaMnO}_3$  and  $\text{LaMnO}_3$  [163,176,177] exhibit various AFM phases that may be conducive to spin current generation and AHE, while Fe-based perovskites, including  $\text{LaFeO}_3$ , and  $\text{YFeO}_3$ , feature G-type AFM ordering [177–180]. Furthermore, fluoride-based perovskites, such as  $\text{NaMnF}_3$ , and  $\text{KMnF}_3$ , also emerge as promising candidates, expanding the range of potential materials for altermagnetic applications [181–183]. Recent first-principles studies by Sattigeri *et al.* [184] highlight the emergence of surface states exhibiting altermagnetic behavior, with spin-splitting believed to be highly dependent on magnetic space groups. The properties of the magnetic surface state have been investigated in three exemplary space groups: orthorhombic ( $Pbnm(62)$ ), hexagonal ( $P6_3/mmc(194)$ ), and tetragonal ( $P4_2/mnm(135)$ ). It was found that the altermagnetic properties on certain surfaces are preserved but annihilated on others because of certain spin-splitting characteristics in the Brillouin zone (BZ). For example,  $\text{LaMnO}_3$  (Space group-62) belonging to the perovskite family with A-type antiferromagnetism, surfaces (010) and (001) are devoid of AM, whereas surface (100) hosts AM with spin splitting of about 30 meV. Furthermore, it was shown that the electric field could have significant control over the surface states and trigger altermagnetism on the otherwise blind surface [184].

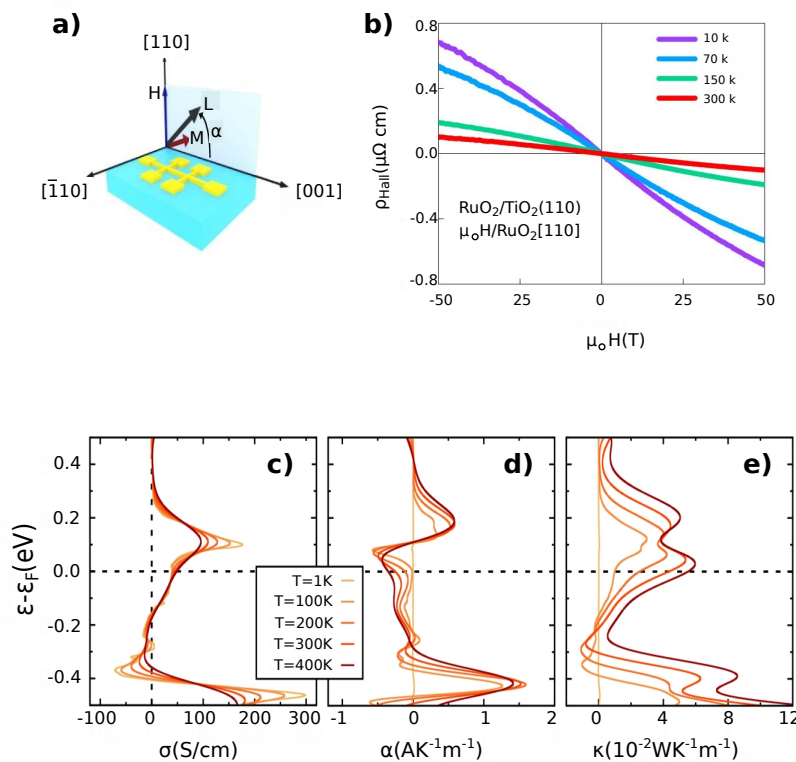


**Figure 7.** Magneto transport measurements. (a) Orientation of the sample along the [110] direction. The red, brown, and black arrows represent the magnetization, Néel vector, and applied field, respectively. (b) Experimental measurement of Hall resistivity with the sample oriented along the [110] direction, respectively. Figures a) and b) are reproduced with permission [185]. Copyright 2022, Springer Nature. (c – e) First-principles simulations of anomalous Hall conductivity  $\sigma$ , anomalous Nernst conductivity  $\alpha$ , and anomalous thermal Hall conductivity  $\kappa$  in a [110]-oriented  $\text{RuO}_2$  film at different temperatures. Figures c–e) are reproduced with permission [186]. Copyright 2024 APS.

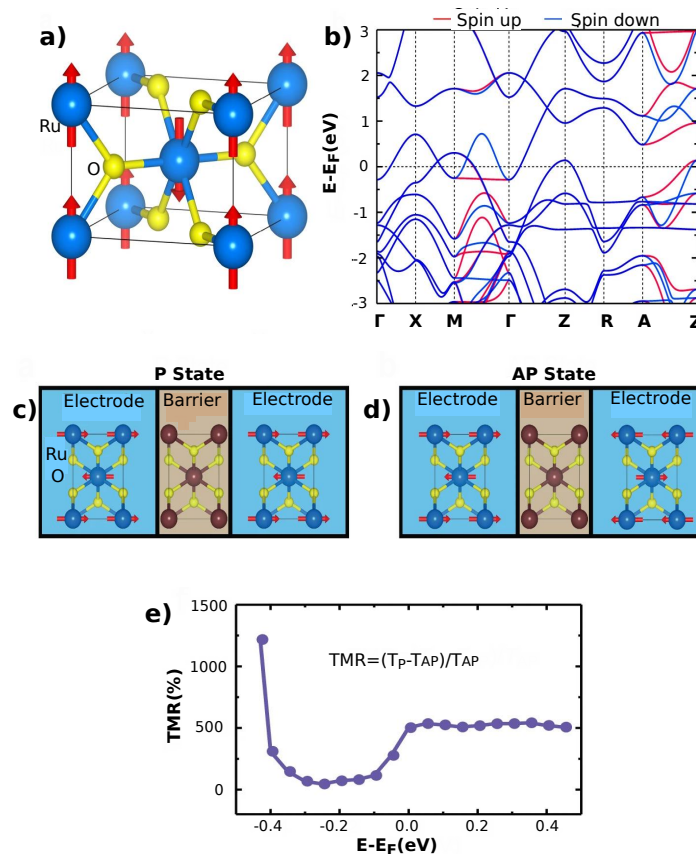


**Figure 8.** a) Tetragonal rutile structure of altermagnetic RuO<sub>2</sub>. b) Band structure of altermagnetic RuO<sub>2</sub> with first principles calculation. c,d) Magnetic tunnel junctions with altermagnetic electrodes. c) Low resistance parallel (P) state. d) Anti-parallel (AP) high resistance state. e) TMR reaching ~ 500% around Fermi level. This figure is reproduced from Ref. [19] under CC-BY 4.0 International License. Published by Springer Nature, copyright 2024.

#### 4.5. Superconductivity and Altermagnets

The observation of altermagnetism in La<sub>2</sub>CuO<sub>4</sub>, which exhibits high temperature superconductivity, has generated significant research interest in the association of superconductivity with AM. [5]. Conventional s-wave superconductivity maintains a uniform Cooper-pair phase around the Fermi surface, akin to ferromagnetism with a single-spin orientation. In contrast, unconventional d-wave superconductivity features a sign-changing Cooper-pair phase, analogous to d-wave magnetism with a sign-changing spin orientation around the Fermi surface [4]. Altermagnetism is suggested to be compatible with spin-triplet superconductivity [187], presenting a valuable opportunity to explore unconventional superconductors that maintain zero stray fields [85]. The unique altermagnetic property enables novel superconducting phenomena in superconductor/altermagnet junctions, including  $0-\pi$  oscillations, multi-nodal current-phase relations, and spin-polarized Andreev levels [33,41,46]. The Josephson effect in AMs differs qualitatively from ferromagnetic junctions, with the decay length and oscillation period influenced by crystallographic orientation [33,46]. AMs also enable tunable superconducting states, such as finite-momentum Cooper pairing and mixed s-wave and p-wave pairings, driven by d-wave altermagnetic order [34,35,41]. They support gapless superconductivity, mirage gaps, and Majorana corner modes under strain or Néel vector rotation, making them promising for cryogenic memory devices and dissipationless superconducting diodes [36,44,51]. The spin-polarized band structure of AMs enables precise control over charge and spin conductance at superconductor interfaces, enhancing functionalities for quantum computing, spintronics, and topological superconductivity [39,47,56].



## 5. Emerging Magneto-Transport Phenomena and Promising Applications

### 5.1. Anomalous Hall Effect

The AHE arises from breaking time-reversal symmetry in magnetic materials, typically due to their intrinsic magnetization and spin-orbit coupling [188]. Therefore, the AHE is also coined as the spontaneous Hall effect, which surprisingly was predicted and observed to occur in non-collinear antiferromagnets [189–195] and, particularly, in AMs [164,185,196–204].

The spontaneous Hall voltage is a phenomenon in which specific internal magnetic configurations cause the electrons to gain transverse velocity. This effect is related to the antisymmetric dissipation-free portion of the conductivity tensor, which is represented by the Hall pseudovector and controls the Hall current [108]. In collinear AFMs, the simplified magnetic structure defined solely by the spin orientations and spatial arrangement of magnetic atoms does not produce a spontaneous Hall conductivity. The necessary asymmetry emerges only when additional atoms, often nonmagnetic, occupy noncentrosymmetric sites. For example, in RuO<sub>2</sub>, the arrangement of oxygen atoms induces an asymmetry in the magnetization density between the two opposing Ru spin sublattices. This breaks the combined symmetry of time-reversal and lattice translation associated with AMs [108], which leads to an additional Hall effect, named the crystal Hall effect, that is independent of the net magnetization or presence of SOC, which highlights a key advantage of AMs [66,201,205]. After initial predictions of a significant AHE in RuO<sub>2</sub> [108], experiments followed quickly with a confirmation [185,199] shown in Figure 7b).

Furthermore, AHE has been observed in altermagnetic thin films of Mn<sub>5</sub>Si<sub>3</sub> [198] and hexagonal MnTe [206]. In the thin film of RuO<sub>2</sub>, one can observe the reorientation of the Néel vector from [001] easy plane to [110] hard plane caused by the application of an electric field, allowing for the observation of AHE [184,194,199].

The detection of the AHE in antiferromagnets, and consequently in AM, offers new possibilities for designing spintronic devices that leverage these materials' robustness and unique properties. Potential applications include high-speed, low-power, and low-dissipative electrical devices as well as innovative quantum computer elements [1–3,207].

### 5.2. Nernst Effects

The Nernst effect is a fundamental phenomenon that emerges in a longitudinal temperature gradient, resulting in a transverse voltage without the application of an external magnetic field. Similar to the AHE, in conventional collinear antiferromagnets, the anomalous Nernst effect (ANE) and the anomalous thermal Hall effect (ATHE) are expected to vanish. However, theoretical work conducted by Zhou *et al.* [186] revealed that significant thermal transport effects exist in RuO<sub>2</sub> (magnetotransport measurements is shown in Figure 7), specifically known as the crystal Nernst effect (CNE) and the crystal thermal Hall effect (CTHE). These effects resemble the ANE and ATHE but are unique to the crystal structure of RuO<sub>2</sub>, where the local environment of the nonmagnetic atom is anisotropic (similar to the discussion of the previous subsection on the AHE) and leads to the emergence of altermagnetism [4]. The study suggests that the sporadic thermal and electrical transport coefficients in RuO<sub>2</sub> adhere to an extended Wiedemann-Franz law in a wide temperature range of (0-150K) [186], a range much wider than what is typically expected for traditional magnetic materials.

As a result, altermagnetic RuO<sub>2</sub> could play a notable role in the realm of spin caloritronics due to its distinct thermal transport properties not attainable by conventional ferromagnets and antiferromagnets. The CNE in RuO<sub>2</sub> shows high anisotropy, which means that its intensity and direction are heavily influenced by the alignment of the Néel vector and can be experimentally observed in films oriented along the directions [110] or [001].

Within RuO<sub>2</sub>, Weyl fermions [208] contribute substantially to Berry curvature. The latter behaves like a magnetic field in the k-space, which impacts electron motion and subsequently affects various transport properties. Weyl fermions are quasi-particles that materialize in substances where electronic bands intersect at discrete points known as Weyl points [209]. The existence of Weyl fermions leads to



significant Berry curvature effects, which are crucial in explaining irregular thermal transport events such as CNE and CTHE. Other sources of Berry curvature include pseudonodal surfaces and ladder transitions. Anomalous transport coefficients can be obtained by integrating the Berry curvature with the BZ [108,186].

### 5.3. Spintronics

A memory device must efficiently read, write, and store data, with magnetoresistance playing a crucial role in ensuring reliable reading. Achieving high magnetoresistance is essential for improving magnetoresistive random access memory (MRAM) reliability, and writing methods typically involve magnetic field-assisted switching or spin-transfer torque (STT)-based writing. Data retention in MRAM is maintained through magnetic anisotropy in the storage layer. Magnetoresistance was first observed in 1856 [210], and its significant enhancement emerged with the introduction of a sandwich structure comprising a free layer, a fixed layer, and a thin non-magnetic spacer. This structure led to the discovery of giant magnetoresistance (GMR) [211,212], where resistance is high when ferromagnetic layers are antiparallel and low when they are parallel, resulting from spin-dependent scattering. A related effect, tunneling magnetoresistance (TMR), was identified in magnetic tunnel junctions (MTJs) at room temperature [213,214]. Unlike GMR, TMR arises from spin-dependent tunneling rather than scattering.

Early MRAM designs relied on magnetic field-induced switching, but this method faced scalability issues since the switching field is inversely proportional to the storage element's size. This limitation was addressed by introducing STT, which enabled field-free switching and improved scalability [215, 216]. In STT, as electrons pass through the fixed layer, minority electrons scatter while majority electrons continue to the free layer, creating polarization. These polarized electrons exert a spin torque on the free layer's magnetization, thereby changing the orientation of magnetization. Enhancing STT efficiency can be achieved by increasing the spin polarization of materials.

Despite its advantages, such as fast switching and non-volatility, STT-MRAM faces challenges like high energy consumption and potential reliability issues. To mitigate these concerns, spin-orbit torque MRAM (SOT-MRAM) was introduced, which separates the read and write paths, significantly improving read reliability and reducing power consumption [217]. However, SOT-MRAM faces material compatibility and fabrication issues [218]. Also, SOT-MRAM relies on relativistic effects, which are spin non-conserving and weaker compared to exchange coupling [20]. In ferromagnets, spin-polarized currents allow spin-dependent effects like STT and GMR/TMR, with resistive changes up to 100% in commercial devices [219–221]. Antiferromagnets, due to their T-invariant spin-degenerate structure, rely on weaker relativistic effects like spin-orbit torque [3,222–225]. With the observation of spin and valley polarization in unconventional AFM materials, significant interest has grown in the AFM spintronics [27]. Ultimately, this led to interest in a new class of materials known as altermagnets (AMs), which exhibit a completely different symmetry compared to conventional antiferromagnets [4, 5].

AMs exhibit strong nonrelativistic T-symmetry breaking and spin splitting despite zero net magnetization. Their spin-dependent anisotropic conductivity enables out-of-plane spin-polarized currents, leading to a GMR effect in altermagnetic multilayers, theoretically reaching  $\sim 100\%$  GMR in  $\text{RuO}_2$  [27]. Additionally, they act as efficient spin splitters, achieving a high charge-spin conversion ratio, surpassing known relativistic spin Hall materials [20,148,226]. This efficiency supports a proposed spin-splitter torque (SST) [20], free from relativistic limitations, with experimental backing [21,23,24].

Altermagnetic tunnel junctions exhibit a TMR effect, with giant TMR predicted with altermagnetic electrode [19,28,29,227,228] shown in Figure 8. Unlike ferromagnets, AMs eliminate stray fields, reducing magnetic cross-talk and enabling simpler device architectures [219,229]. Their high-frequency (THz-range) spin dynamics facilitate ultrafast, low-energy switching, approaching the Landauer energy limit [230–235]

## 6. Conclusions

To summarize, altermagnetism is an appealing, novel, and distinct magnetic phase possessing zero net magnetization and strong time-reversal symmetry-breaking responses. It expands the traditional understanding of magnetism, which was previously limited to ferromagnetism and antiferromagnetism. The theoretical framework based on symmetry principles to classify and describe altermagnetism offers a clear distinction between ferromagnetic, antiferromagnetic, and altermagnetic phases.

Candidate altermagnetic materials range from insulators to superconductors as initially predicted by Smejkal *et al.* [4] and were followed by several subsequent studies (see, e.g., Refs. [72,96,110,112,150]). Such predictions associated with state-of-the-art experiments are essential for guiding future research activities and exploring the technological application of altermagnetic materials in information technology by harnessing emerging spintronics phenomena, ultrafast photomagnetism, and thermoelectrics [19,54,236]. There is a need for more experimental investigations to identify altermagnetic materials. Various stacking and twisting of van der Waals systems can be experimentally achieved [237–243]. Techniques such as nano/micro ARPES enable direct probing of the electronic properties of twisted van der Waals layers [71,244,245], while the magneto-optic Kerr effect (MOKE) provides a reliable method for detecting time-reversal symmetry breaking [246–248]. The special properties of altermagnetism, including strong NRSS and high magnetic ordering temperatures, make them promising candidates for next-generation devices. AMs can operate in the THz range and exhibit nondegenerate magnonic chirality without external fields [129], offering potential for the development of energy-efficient magnon spintronics devices [249]. Despite growing interest in their potential applications, further research is essential to bridge the gap between theoretical predictions and practical implementation.

**Acknowledgments:** DPR acknowledges the Science & Engineering Research Board (SERB), New Delhi Govt. of India via File Number: SIR/2022/001150. RT acknowledges the University Grants Commission (UGC), India, for the Junior Research Fellowship (JRF), ID No. 231620066332.

## References

1. Baltz, V.; Manchon, A.; Tsoi, M.; Moriyama, T.; Ono, T.; Tserkovnyak, Y. Antiferromagnetic spintronics. *Reviews of Modern Physics* **2018**, *90*, 015005.
2. Khalili Amiri, P.; Phatak, C.; Finocchio, G. Prospects for Antiferromagnetic Spintronic Devices. *Annual Review of Materials Research* **2024**, *54*.
3. Jungwirth, T.; Marti, X.; Wadley, P.; Wunderlich, J. Antiferromagnetic spintronics. *Nature nanotechnology* **2016**, *11*, 231–241.
4. Šmejkal, L.; Sinova, J.; Jungwirth, T. Emerging research landscape of altermagnetism. *Physical Review X* **2022**, *12*, 040501.
5. Šmejkal, L.; Sinova, J.; Jungwirth, T. Beyond conventional ferromagnetism and antiferromagnetism: A phase with nonrelativistic spin and crystal rotation symmetry. *Physical Review X* **2022**, *12*, 031042.
6. Mazin, I.; Editors, P. Altermagnetism—a new punch line of fundamental magnetism, 2022.
7. Néel, L. Some new results on antiferromagnetism and ferromagnetism. *Reviews of Modern Physics* **1953**, *25*, 58.
8. Rashba, E.I. Spin-orbit coupling in condensed matter physics. *Sov. Phys. Solid State* **1960**, *2*, 1109.
9. Dresselhaus, G. Spin-orbit coupling effects in zinc blende structures. *Physical Review* **1955**, *100*, 580.
10. Yuan, L.D.; Wang, Z.; Luo, J.W.; Rashba, E.I.; Zunger, A. Giant momentum-dependent spin splitting in centrosymmetric low-Z antiferromagnets. *Physical Review B* **2020**, *102*, 014422.
11. Jungwirth, T.; Fernandes, R.M.; Sinova, J.; Smejkal, L. Altermagnets and beyond: Nodal magnetically-ordered phases. *arXiv preprint arXiv:2409.10034* **2024**.
12. Gomonay, O.; Kravchuk, V.; Jaeschke-Ubiergo, R.; Yershov, K.; Jungwirth, T.; Šmejkal, L.; Brink, J.v.d.; Sinova, J. Structure, control, and dynamics of altermagnetic textures. *npj Spintronics* **2024**, *2*, 35.
13. Pomeranchuk, I.I.; et al. On the stability of a Fermi liquid. *Sov. Phys. JETP* **1958**, *8*, 361.
14. Wu, C.; Sun, K.; Fradkin, E.; Zhang, S.C. Fermi liquid instabilities in the spin channel. *Physical Review B—Condensed Matter and Materials Physics* **2007**, *75*, 115103.

15. Cheong, S.W.; Huang, F.T. Altermagnetism with non-collinear spins. *npj Quantum Materials* **2024**, *9*, 13.
16. Smolyanyuk, A.; Šmejkal, L.; Mazin, I.I. A tool to check whether a symmetry-compensated collinear magnetic material is antiferro-or altermagnetic. *SciPost Physics Codebases* **2024**, p. 030.
17. Bai, L.; Feng, W.; Liu, S.; Šmejkal, L.; Mokrousov, Y.; Yao, Y. Altermagnetism: Exploring new frontiers in magnetism and spintronics. *Advanced Functional Materials* **2024**, p. 2409327.
18. Gao, Z.F.; Qu, S.; Zeng, B.; Wen, J.R.; Sun, H.; Guo, P.; Lu, Z.Y. Ai-accelerated discovery of altermagnetic materials. *arXiv preprint arXiv:2311.04418* **2023**.
19. Shao, D.F.; Zhang, S.H.; Li, M.; Eom, C.B.; Tsymbal, E.Y. Spin-neutral currents for spintronics. *Nature Communications* **2021**, *12*, 7061.
20. González-Hernández, R.; Šmejkal, L.; Vybírný, K.; Yahagi, Y.; Sinova, J.; Jungwirth, T.; Železný, J. Efficient electrical spin splitter based on nonrelativistic collinear antiferromagnetism. *Physical Review Letters* **2021**, *126*, 127701.
21. Bose, A.; Schreiber, N.J.; Jain, R.; Shao, D.F.; Nair, H.P.; Sun, J.; Zhang, X.S.; Muller, D.A.; Tsymbal, E.Y.; Schlom, D.G.; et al. Tilted spin current generated by the collinear antiferromagnet ruthenium dioxide. *Nature Electronics* **2022**, *5*, 267–274.
22. Naka, M.; Motome, Y.; Seo, H. Perovskite as a spin current generator. *Physical Review B* **2021**, *103*, 125114.
23. Bai, H.; Han, L.; Feng, X.; Zhou, Y.; Su, R.; Wang, Q.; Liao, L.; Zhu, W.; Chen, X.; Pan, F.; et al. Observation of spin splitting torque in a collinear antiferromagnet RuO<sub>2</sub>. *Physical Review Letters* **2022**, *128*, 197202.
24. Karube, S.; Tanaka, T.; Sugawara, D.; Kadoguchi, N.; Kohda, M.; Nitta, J. Observation of spin-splitter torque in collinear antiferromagnetic RuO<sub>2</sub>. *Physical review letters* **2022**, *129*, 137201.
25. Bai, H.; Zhang, Y.; Zhou, Y.; Chen, P.; Wan, C.; Han, L.; Zhu, W.; Liang, S.; Su, Y.; Han, X.; et al. Efficient spin-to-charge conversion via altermagnetic spin splitting effect in antiferromagnet RuO<sub>2</sub>. *Physical review letters* **2023**, *130*, 216701.
26. Zhang, Y.; Bai, H.; Han, L.; Chen, C.; Zhou, Y.; Back, C.H.; Pan, F.; Wang, Y.; Song, C. Simultaneous High Charge-Spin Conversion Efficiency and Large Spin Diffusion Length in Altermagnetic RuO<sub>2</sub>. *Advanced Functional Materials* **2024**, *34*, 2313332.
27. Šmejkal, L.; Hellenes, A.B.; González-Hernández, R.; Sinova, J.; Jungwirth, T. Giant and tunneling magnetoresistance in unconventional collinear antiferromagnets with nonrelativistic spin-momentum coupling. *Physical Review X* **2022**, *12*, 011028.
28. Jiang, Y.Y.; Wang, Z.A.; Samanta, K.; Zhang, S.H.; Xiao, R.C.; Lu, W.; Sun, Y.; Tsymbal, E.Y.; Shao, D.F. Prediction of giant tunneling magnetoresistance in RuO<sub>2</sub>/TiO<sub>2</sub>/RuO<sub>2</sub> (110) antiferromagnetic tunnel junctions. *Physical Review B* **2023**, *108*, 174439.
29. Chi, B.; Jiang, L.; Zhu, Y.; Yu, G.; Wan, C.; Zhang, J.; Han, X. Crystal-facet-oriented altermagnets for detecting ferromagnetic and antiferromagnetic states by giant tunneling magnetoresistance. *Physical Review Applied* **2024**, *21*, 034038.
30. Das, S.; Suri, D.; Soori, A. Transport across junctions of altermagnets with normal metals and ferromagnets. *Journal of Physics: Condensed Matter* **2023**, *35*, 435302.
31. Gonzalez Betancourt, R.D.; Zubáč, J.; Geishendorf, K.; Ritzinger, P.; Růžicková, B.; Kotte, T.; Železný, J.; Olejník, K.; Springholz, G.; Büchner, B.; et al. Anisotropic magnetoresistance in altermagnetic MnTe. *npj Spintronics* **2024**, *2*, 45.
32. Liu, F.; Zhang, Z.; Yuan, X.; Liu, Y.; Zhu, S.; Lu, Z.; Xiong, R. Giant tunneling magnetoresistance in insulated altermagnet/ferromagnet junctions induced by spin-dependent tunneling effect. *Physical Review B* **2024**, *110*, 134437.
33. Ouassou, J.A.; Brataas, A.; Linder, J. dc Josephson effect in altermagnets. *Physical review letters* **2023**, *131*, 076003.
34. Zhu, D.; Zhuang, Z.Y.; Wu, Z.; Yan, Z. Topological superconductivity in two-dimensional altermagnetic metals. *Physical Review B* **2023**, *108*, 184505.
35. Zhang, S.B.; Hu, L.H.; Neupert, T. Finite-momentum Cooper pairing in proximitized altermagnets. *Nature Communications* **2024**, *15*, 1801.
36. Li, Y.X.; Liu, C.C. Majorana corner modes and tunable patterns in an altermagnet heterostructure. *Physical Review B* **2023**, *108*, 205410.
37. Papaj, M. Andreev reflection at the altermagnet-superconductor interface. *Physical Review B* **2023**, *108*, L060508.
38. Banerjee, S.; Scheurer, M.S. Altermagnetic superconducting diode effect. *Physical Review B* **2024**, *110*, 024503.
39. Sun, C.; Brataas, A.; Linder, J. Andreev reflection in altermagnets. *Physical Review B* **2023**, *108*, 054511.

40. Brekke, B.; Brataas, A.; Sudbø, A. Two-dimensional altermagnets: Superconductivity in a minimal microscopic model. *Physical Review B* **2023**, *108*, 224421.
41. Beenakker, C.; Vakhtel, T. Phase-shifted Andreev levels in an altermagnet Josephson junction. *Physical Review B* **2023**, *108*, 075425.
42. Chakraborty, D.; Black-Schaffer, A.M. Zero-field finite-momentum and field-induced superconductivity in altermagnets. *Physical Review B* **2024**, *110*, L060508.
43. Cheng, Q.; Sun, Q.F. Orientation-dependent Josephson effect in spin-singlet superconductor/altermagnet/spin-triplet superconductor junctions. *Physical Review B* **2024**, *109*, 024517.
44. Giil, H.G.; Linder, J. Superconductor-altermagnet memory functionality without stray fields. *Physical Review B* **2024**, *109*, 134511.
45. Zyuzin, A.A. Magnetoelectric effect in superconductors with d-wave magnetization. *Physical Review B* **2024**, *109*, L220505.
46. Lu, B.; Maeda, K.; Ito, H.; Yada, K.; Tanaka, Y.  $\varphi$  Josephson junction induced by altermagnetism. *Physical Review Letters* **2024**, *133*, 226002.
47. Wei, M.; Xiang, L.; Xu, F.; Zhang, L.; Tang, G.; Wang, J. Gapless superconducting state and mirage gap in altermagnets. *Physical Review B* **2024**, *109*, L201404.
48. Bose, A.; Vadnais, S.; Paramakanti, A. Altermagnetism and superconductivity in a multiorbital t-J model. *Physical Review B* **2024**, *110*, 205120.
49. Mæland, K.; Brekke, B.; Sudbø, A. Many-body effects on superconductivity mediated by double-magnon processes in altermagnets. *Physical Review B* **2024**, *109*, 134515.
50. Sumita, S.; Naka, M.; Seo, H. Fulde-Ferrell-Larkin-Ovchinnikov state induced by antiferromagnetic order in  $\kappa$ -type organic conductors. *Physical Review Research* **2023**, *5*, 043171.
51. Cheng, Q.; Mao, Y.; Sun, Q.F. Field-free Josephson diode effect in altermagnet/normal metal/altermagnet junctions. *Physical Review B* **2024**, *110*, 014518.
52. Das, S.; Soori, A. Crossed Andreev reflection in altermagnets. *Physical Review B* **2024**, *109*, 245424.
53. Hu, J.X.; Matsyshyn, O.; Song, J.C. Nonlinear superconducting magnetoelectric effect. *Physical Review Letters* **2025**, *134*, 026001.
54. Sukhachov, P.O.; Hodt, E.W.; Linder, J. Thermoelectric effect in altermagnet-superconductor junctions. *Physical Review B* **2024**, *110*, 094508.
55. Li, Y.X. Realizing tunable higher-order topological superconductors with altermagnets. *Physical Review B* **2024**, *109*, 224502.
56. Niu, Z.P.; Zhang, Y.M. Electrically controlled crossed Andreev reflection in altermagnet/superconductor/altermagnet junctions. *Superconductor Science and Technology* **2024**, *37*, 055012.
57. Niu, Z.P.; Yang, Z. Orientation-dependent Andreev reflection in an altermagnet/altermagnet/superconductor junction. *Journal of Physics D: Applied Physics* **2024**, *57*, 395301.
58. Baltz, V.; Hoffmann, A.; Emori, S.; Shao, D.F.; Jungwirth, T. Emerging materials in antiferromagnetic spintronics. *APL Materials* **2024**, *12*.
59. Qiu, H.; Seifert, T.S.; Huang, L.; Zhou, Y.; Kašpar, Z.; Zhang, C.; Wu, J.; Fan, K.; Zhang, Q.; Wu, D.; et al. Terahertz spin current dynamics in antiferromagnetic hematite. *Advanced Science* **2023**, *10*, 2300512.
60. Reichlova, H.; Kriegner, D.; Mook, A.; Althammer, M.; Thomas, A. Role of topology in compensated magnetic systems. *APL Materials* **2024**, *12*.
61. Li, Y.X.; Liu, Y.; Liu, C.C. Creation and manipulation of higher-order topological states by altermagnets. *Physical Review B* **2024**, *109*, L201109.
62. Ghorashi, S.A.A.; Hughes, T.L.; Cano, J. Altermagnetic routes to Majorana modes in zero net magnetization. *Physical review letters* **2024**, *133*, 106601.
63. Yan, H.; Zhou, X.; Qin, P.; Liu, Z. Review on spin-split antiferromagnetic spintronics. *Applied Physics Letters* **2024**, *124*.
64. Kang, W.; Zhang, Y.; Wang, Z.; Klein, J.O.; Chappert, C.; Ravelosona, D.; Wang, G.; Zhang, Y.; Zhao, W. Spintronics: Emerging ultra-low-power circuits and systems beyond MOS technology. *ACM Journal on Emerging Technologies in Computing Systems (JETC)* **2015**, *12*, 1–42.
65. Joshi, V.K. Spintronics: A contemporary review of emerging electronics devices. *Engineering science and technology, an international journal* **2016**, *19*, 1503–1513.
66. McClarty, P.A.; Rau, J.G. Landau theory of altermagnetism. *Physical Review Letters* **2024**, *132*, 176702.
67. Litvin, D.B. Spin point groups. *Acta Crystallographica Section A: Crystal Physics, Diffraction, Theoretical and General Crystallography* **1977**, *33*, 279–287.



68. Litvin, D.B.; Opechowski, W. Spin groups. *Physica* **1974**, *76*, 538–554.
69. Hertz, H. Ueber sehr schnelle elektrische Schwingungen. *Annalen der Physik* **1887**, *267*, 421–448.
70. Einstein, A. Über einen die Erzeugung und Verwandlung des Lichtes betreffenden heuristischen Gesichtspunkt, 1905.
71. Zhang, H.; Pincelli, T.; Jozwiak, C.; Kondo, T.; Ernstorfer, R.; Sato, T.; Zhou, S. Angle-resolved photoemission spectroscopy. *Nature Reviews Methods Primers* **2022**, *2*, 54.
72. Lee, S.; Lee, S.; Jung, S.; Jung, J.; Kim, D.; Lee, Y.; Seok, B.; Kim, J.; Park, B.G.; Šmejkal, L.; et al. Broken kramers degeneracy in altermagnetic mnite. *Physical Review Letters* **2024**, *132*, 036702.
73. Saitoh, Y.; Kimura, H.; Suzuki, Y.; Nakatani, T.; Matsushita, T.; Muro, T.; Miyahara, T.; Fujisawa, M.; Soda, K.; Ueda, S.; et al. Performance of a very high resolution soft x-ray beamline BL25SU with a twin-helical undulator at SPring-8. *Review of Scientific Instruments* **2000**, *71*, 3254–3259.
74. Borisenko, S.V. “One-cubed” ARPES user facility at BESSY II. *Synchrotron Radiation News* **2012**, *25*, 6–11.
75. Reininger, R.; Hulbert, S.; Johnson, P.; Sadowski, J.; Starr, D.; Chubar, O.; Valla, T.; Vescovo, E. The electron spectro-microscopy beamline at National Synchrotron Light Source II: A wide photon energy range, micro-focusing beamline for photoelectron spectro-microscopies. *Review of Scientific Instruments* **2012**, *83*.
76. Tamura, L.; Hussain, Z.; Padmore, H.; Robin, D.; Bailey, S.; Feinberg, B.; Falcone, R. Advanced light source update. *Synchrotron Radiation News* **2012**, *25*, 25–30.
77. Strocov, V.; Wang, X.; Shi, M.; Kobayashi, M.; Krempasky, J.; Hess, C.; Schmitt, T.; Patthey, L. Soft-X-ray ARPES facility at the ADRESS beamline of the SLS: concepts, technical realisation and scientific applications. *Synchrotron Radiation* **2014**, *21*, 32–44.
78. Hoesch, M.; Kim, T.; Dudin, P.; Wang, H.; Scott, S.; Harris, P.; Patel, S.; Matthews, M.; Hawkins, D.; Alcock, S.; et al. A facility for the analysis of the electronic structures of solids and their surfaces by synchrotron radiation photoelectron spectroscopy. *Review of Scientific Instruments* **2017**, *88*.
79. Sekiyama, A.; Iwasaki, T.; Matsuda, K.; Saitoh, Y.; Onuki, Y.; Suga, S. Probing bulk states of correlated electron systems by high-resolution resonance photoemission. *Nature* **2000**, *403*, 396–398.
80. Fadley, C.S. Looking deeper: angle-resolved photoemission with soft and hard X-rays. *Synchrotron Radiation News* **2012**, *25*, 26–31.
81. Ding, J.; Jiang, Z.; Chen, X.; Tao, Z.; Liu, Z.; Li, T.; Liu, J.; Sun, J.; Cheng, J.; Liu, J.; et al. Large Band Splitting in g-Wave Altermagnet CrSb. *Physical Review Letters* **2024**, *133*, 206401.
82. Moser, S. An experimentalist’s guide to the matrix element in angle resolved photoemission. *Journal of Electron Spectroscopy and Related Phenomena* **2017**, *214*, 29–52.
83. Ohtomo, A.; Hwang, H. A high-mobility electron gas at the LaAlO<sub>3</sub>/SrTiO<sub>3</sub> heterointerface. *Nature* **2004**, *427*, 423–426.
84. Reyren, N.; Thiel, S.; Caviglia, A.; Kourkoutis, L.F.; Hammerl, G.; Richter, C.; Schneider, C.W.; Kopp, T.; Ruetschi, A.S.; Jaccard, D.; et al. Superconducting interfaces between insulating oxides. *Science* **2007**, *317*, 1196–1199.
85. Song, C.; Bai, H.; Zhou, Z.; Han, L.; Reichlova, H.; Dil, J.H.; Liu, J.; Chen, X.; Pan, F. Altermagnets as a new class of functional materials. *Nature Reviews Materials* **2025**, pp. 1–13.
86. Nemšák, S.; Conti, G.; Gray, A.; Palsson, G.; Conlon, C.; Eiteneer, D.; Keqi, A.; Rattanachata, A.; Saw, A.; Bostwick, A.; et al. Energetic, spatial, and momentum character of the electronic structure at a buried interface: The two-dimensional electron gas between two metal oxides. *Physical Review B* **2016**, *93*, 245103.
87. Berner, G.; Sing, M.; Pfaff, F.; Benckiser, E.; Wu, M.; Christiani, G.; Logvenov, G.; Habermeier, H.U.; Kobayashi, M.; Strocov, V.; et al. Dimensionality-tuned electronic structure of nickelate superlattices explored by soft-x-ray angle-resolved photoelectron spectroscopy. *Physical Review B* **2015**, *92*, 125130.
88. Reimers, S.; Odenbreit, L.; Šmejkal, L.; Strocov, V.N.; Constantinou, P.; Hellenes, A.B.; Jaeschke Ubierto, R.; Campos, W.H.; Bharadwaj, V.K.; Chakraborty, A.; et al. Direct observation of altermagnetic band splitting in CrSb thin films. *Nature Communications* **2024**, *15*, 2116.
89. Yang, G.; Li, Z.; Yang, S.; Li, J.; Zheng, H.; Zhu, W.; Pan, Z.; Xu, Y.; Cao, S.; Zhao, W.; et al. Three-dimensional mapping of the altermagnetic spin splitting in CrSb. *Nature Communications* **2025**, *16*, 1442.
90. Zeng, M.; Zhu, M.Y.; Zhu, Y.P.; Liu, X.R.; Ma, X.M.; Hao, Y.J.; Liu, P.; Qu, G.; Yang, Y.; Jiang, Z.; et al. Observation of Spin Splitting in Room-Temperature Metallic Antiferromagnet CrSb. *Advanced Science* **2024**, p. 2406529.
91. Jozwiak, C.; Graf, J.; Lebedev, G.; Andresen, N.; Schmid, A.; Fedorov, A.; El Gabaly, F.; Wan, W.; Lanzara, A.; Hussain, Z. A high-efficiency spin-resolved photoemission spectrometer combining time-of-flight spectroscopy with exchange-scattering polarimetry. *Review of Scientific Instruments* **2010**, *81*.



92. Okuda, T. Recent trends in spin-resolved photoelectron spectroscopy. *Journal of Physics: Condensed Matter* **2017**, *29*, 483001.
93. Lin, C.Y.; Moreschini, L.; Lanzara, A. Present and future trends in spin ARPES. *Europhysics Letters* **2021**, *134*, 57001.
94. Krempaský, J.; Šmejkal, L.; D'souza, S.; Hajlaoui, M.; Springholz, G.; Uhlířová, K.; Alarab, F.; Constantinou, P.; Strocov, V.; Usanov, D.; et al. Altermagnetic lifting of Kramers spin degeneracy. *Nature* **2024**, *626*, 517–522.
95. Liu, J.; Zhan, J.; Li, T.; Liu, J.; Cheng, S.; Shi, Y.; Deng, L.; Zhang, M.; Li, C.; Ding, J.; et al. Absence of Altermagnetic Spin Splitting Character in Rutile Oxide RuO<sub>2</sub>. *Physical Review Letters* **2024**, *133*, 176401.
96. Osumi, T.; Souma, S.; Aoyama, T.; Yamauchi, K.; Honma, A.; Nakayama, K.; Takahashi, T.; Ohgushi, K.; Sato, T. Observation of a giant band splitting in altermagnetic MnTe. *Physical Review B* **2024**, *109*, 115102.
97. Zhu, Y.P.; Chen, X.; Liu, X.R.; Liu, Y.; Liu, P.; Zha, H.; Qu, G.; Hong, C.; Li, J.; Jiang, Z.; et al. Observation of plaid-like spin splitting in a noncoplanar antiferromagnet. *Nature* **2024**, *626*, 523–528.
98. Lin, Z.; Chen, D.; Lu, W.; Liang, X.; Feng, S.; Yamagami, K.; Osiecki, J.; Leandersson, M.; Thiagarajan, B.; Liu, J.; et al. Observation of giant spin splitting and d-wave spin texture in room temperature altermagnet ruo<sub>2</sub>. *arXiv preprint arXiv:2402.04995* **2024**.
99. Zhang, F.; Cheng, X.; Yin, Z.; Liu, C.; Deng, L.; Qiao, Y.; Shi, Z.; Zhang, S.; Lin, J.; Liu, Z.; et al. Crystal-symmetry-paired spin-valley locking in a layered room-temperature antiferromagnet. *arXiv preprint arXiv:2407.19555* **2024**.
100. Jiang, B.; Hu, M.; Bai, J.; Song, Z.; Mu, C.; Qu, G.; Li, W.; Zhu, W.; Pi, H.; Wei, Z.; et al. A metallic room-temperature d-wave altermagnet. *Nature Physics* **2025**, pp. 1–6.
101. Phillips, C.; Pokharel, G.; Shtefiienko, K.; Bhandari, S.R.; Graf, D.E.; Rai, D.; Shrestha, K. Electronic structure of the altermagnet candidate FeSb<sub>2</sub>: High-field torque magnetometry and density functional theory studies. *Physical Review B* **2025**, *111*, 075141.
102. Keßler, P.; Garcia-Gassull, L.; Suter, A.; Prokscha, T.; Salman, Z.; Khalyavin, D.; Manuel, P.; Orlandi, F.; Mazin, I.I.; Valentí, R.; et al. Absence of magnetic order in RuO<sub>2</sub>: insights from  $\mu$  SR spectroscopy and neutron diffraction. *npj Spintronics* **2024**, *2*, 50.
103. Lovesey, S.; Khalyavin, D.; Van Der Laan, G. Templates for magnetic symmetry and altermagnetism in hexagonal MnTe. *Physical Review B* **2023**, *108*, 174437.
104. Hariki, A.; Okauchi, T.; Takahashi, Y.; Kuneš, J. Determination of the Néel vector in rutile altermagnets through x-ray magnetic circular dichroism: The case of MnF<sub>2</sub>. *Physical Review B* **2024**, *110*, L100402.
105. Hariki, A.; Takahashi, Y.; Kuneš, J. X-ray magnetic circular dichroism in RuO<sub>2</sub>. *Physical Review B* **2024**, *109*, 094413.
106. Amin, O.; Dal Din, A.; Golias, E.; Niu, Y.; Zakharov, A.; Fromage, S.; Fields, C.; Heywood, S.; Cousins, R.; Maccherozzi, F.; et al. Nanoscale imaging and control of altermagnetism in MnTe. *Nature* **2024**, *636*, 348–353.
107. Hariki, A.; Dal Din, A.; Amin, O.; Yamaguchi, T.; Badura, A.; Kriegner, D.; Edmonds, K.; Champion, R.; Wadley, P.; Backes, D.; et al. X-ray magnetic circular dichroism in altermagnetic  $\alpha$ -MnTe. *Physical Review Letters* **2024**, *132*, 176701.
108. Šmejkal, L.; González-Hernández, R.; Jungwirth, T.; Sinova, J. Crystal time-reversal symmetry breaking and spontaneous Hall effect in collinear antiferromagnets. *Science advances* **2020**, *6*, eaaz8809.
109. Ahn, K.H.; Hariki, A.; Lee, K.W.; Kuneš, J. Antiferromagnetism in RuO<sub>2</sub> as d-wave Pomeranchuk instability. *Physical Review B* **2019**, *99*, 184432.
110. Bhowal, S.; Spaldin, N.A. Ferroically Ordered Magnetic Octupoles in d-Wave Altermagnets. *Phys. Rev. X* **2024**, *14*, 011019. <https://doi.org/10.1103/PhysRevX.14.011019>.
111. Yuan, L.D.; Wang, Z.; Luo, J.W.; Zunger, A. Prediction of low-Z collinear and noncollinear antiferromagnetic compounds having momentum-dependent spin splitting even without spin-orbit coupling. *Physical Review Materials* **2021**, *5*, 014409.
112. Guo, Y.; Liu, H.; Janson, O.; Fulga, I.C.; van den Brink, J.; Facio, J.I. Spin-split collinear antiferromagnets: A large-scale ab-initio study. *Materials Today Physics* **2023**, *32*, 100991.
113. Nag, J.; Das, B.; Bhowal, S.; Nishioka, Y.; Bandyopadhyay, B.; Sarker, S.; Kumar, S.; Kuroda, K.; Gopalan, V.; Kimura, A.; et al. GdAlSi: An antiferromagnetic topological Weyl semimetal with nonrelativistic spin splitting. *Physical Review B* **2024**, *110*, 224436.
114. Fedchenko, O.; Minár, J.; Akashdeep, A.; D'Souza, S.W.; Vasilyev, D.; Tkach, O.; Odenbreit, L.; Nguyen, Q.; Kutnyakhov, D.; Wind, N.; et al. Observation of time-reversal symmetry breaking in the band structure of altermagnetic RuO<sub>2</sub>. *Science advances* **2024**, *10*, eadj4883.

115. Dale, N.; Ashour, O.A.; Vila, M.; Regmi, R.B.; Fox, J.; Johnson, C.W.; Fedorov, A.; Stibor, A.; Ghimire, N.J.; Griffin, S.M. Non-relativistic spin splitting above and below the Fermi level in a g-wave altermagnet. *arXiv preprint arXiv:2411.18761* **2024**.
116. Sakhya, A.P.; Mondal, M.I.; Sprague, M.; Regmi, R.B.; Kumay, A.K.; Sheokand, H.; Mazin, I.; Ghimire, N.J.; Neupane, M.; et al. Electronic structure of a layered altermagnetic compound CoNb<sub>4</sub>Se<sub>8</sub>. *arXiv preprint arXiv:2503.16670* **2025**.
117. De Vita, A.; Bigi, C.; Romanin, D.; Watson, M.D.; Polewczyk, V.; Zonno, M.; Bertran, F.; Petersen, M.B.; Motti, F.; Vinai, G.; et al. Optical switching in a layered altermagnet. *arXiv preprint arXiv:2502.20010* **2025**.
118. Candelora, C.; Xu, M.; Cheng, S.; De Vita, A.; Romanin, D.; Bigi, C.; Petersen, M.B.; LaFleur, A.; Calandra, M.; Miwa, J.; et al. Discovery of intertwined spin and charge density waves in a layered altermagnet. *arXiv preprint arXiv:2503.03716* **2025**.
119. Ryden, W.; Lawson, A. Magnetic susceptibility of IrO<sub>2</sub> and RuO<sub>2</sub>. *The Journal of Chemical Physics* **1970**, *52*, 6058–6061.
120. Berlijn, T.; Snijders, P.C.; Delaire, O.; Zhou, H.D.; Maier, T.A.; Cao, H.B.; Chi, S.X.; Matsuda, M.; Wang, Y.; Koehler, M.R.; et al. Itinerant antiferromagnetism in RuO<sub>2</sub>. *Physical review letters* **2017**, *118*, 077201.
121. Zhu, Z.; Stremper, J.; Rao, R.; Occhialini, C.; Pellicciari, J.; Choi, Y.; Kawaguchi, T.; You, H.; Mitchell, J.; Shao-Horn, Y.; et al. Anomalous antiferromagnetism in metallic RuO<sub>2</sub> determined by resonant X-ray scattering. *Physical review letters* **2019**, *122*, 017202.
122. Smolyanyuk, A.; Mazin, I.I.; Garcia-Gassull, L.; Valentí, R. Fragility of the magnetic order in the prototypical altermagnet RuO<sub>2</sub>. *Physical Review B* **2024**, *109*, 134424.
123. Brahim, S.; Rai, D.P.; Lounis, S. Confinement-induced altermagnetism in RuO<sub>2</sub> ultrathin films. *ArXiv*: **2024**, 2412.15377.
124. Jeong, S.G.; Choi, I.H.; Nair, S.; Buiarelli, L.; Pourbahari, B.; Oh, J.Y.; Bassim, N.; Seo, A.; Choi, W.S.; Fernandes, R.M.; et al. Altermagnetic polar metallic phase in ultra-thin epitaxially-strained RuO<sub>2</sub> films. *arXiv preprint arXiv:2405.05838* **2024**.
125. Weber, M.; Wust, S.; Haag, L.; Akashdeep, A.; Leckron, K.; Schmitt, C.; Ramos, R.; Kikkawa, T.; Saitoh, E.; Kläui, M.; et al. All optical excitation of spin polarization in d-wave altermagnets. *arXiv preprint arXiv:2408.05187* **2024**.
126. Reichlova, H.; Lopes Seeger, R.; González-Hernández, R.; Kounta, I.; Schlitz, R.; Kriegner, D.; Ritzinger, P.; Lammel, M.; Leiviskä, M.; Birk Hellenes, A.; et al. Observation of a spontaneous anomalous Hall response in the Mn<sub>5</sub>Si<sub>3</sub> d-wave altermagnet candidate. *Nature Communications* **2024**, *15*, 4961.
127. Han, L.; Fu, X.; Peng, R.; Cheng, X.; Dai, J.; Liu, L.; Li, Y.; Zhang, Y.; Zhu, W.; Bai, H.; et al. Electrical 180 switching of Néel vector in spin-splitting antiferromagnet. *Science Advances* **2024**, *10*, eadn0479.
128. Hiraishi, M.; Okabe, H.; Koda, A.; Kadono, R.; Muroi, T.; Hirai, D.; Hiroi, Z. Nonmagnetic Ground State in RuO<sub>2</sub> Revealed by Muon Spin Rotation. *Physical Review Letters* **2024**, *132*, 166702.
129. Šmejkal, L.; Marmodoro, A.; Ahn, K.H.; González-Hernández, R.; Turek, I.; Mankovsky, S.; Ebert, H.; D'Souza, S.W.; Šipr, O.; Sinova, J.; et al. Chiral magnons in altermagnetic RuO<sub>2</sub>. *Physical Review Letters* **2023**, *131*, 256703.
130. Gohlke, M.; Corticelli, A.; Moessner, R.; McClarty, P.A.; Mook, A. Spurious symmetry enhancement in linear spin wave theory and interaction-induced topology in magnons. *Physical Review Letters* **2023**, *131*, 186702.
131. Kumar, D.; Jin, T.; Sbiaa, R.; Kläui, M.; Bedanta, S.; Fukami, S.; Ravelosona, D.; Yang, S.H.; Liu, X.; Piramanayagam, S. Domain wall memory: Physics, materials, and devices. *Physics Reports* **2022**, *958*, 1–35.
132. Pan, B.; Zhou, P.; Lyu, P.; Xiao, H.; Yang, X.; Sun, L. General Stacking Theory for Altermagnetism in Bilayer Systems. *Physical Review Letters* **2024**, *133*, 166701.
133. Zhu, Y.; Chen, T.; Li, Y.; Qiao, L.; Ma, X.; Liu, C.; Hu, T.; Gao, H.; Ren, W. Multipiezo effect in altermagnetic V<sub>2</sub>SeTeO monolayer. *Nano Letters* **2023**, *24*, 472–478.
134. Sun, W.; Ye, H.; Liang, L.; Ding, N.; Dong, S.; Wang, S.S. Stacking-dependent ferroicity of a reversed bilayer: Altermagnetism or ferroelectricity. *Physical Review B* **2024**, *110*, 224418.
135. Liu, Q.; Kang, J.; Wang, P.; Gao, W.; Qi, Y.; Zhao, J.; Jiang, X. Inverse Magnetocaloric Effect in Altermagnetic 2D Non-van der Waals FeX (X= S and Se) Semiconductors. *Advanced Functional Materials* **2024**, p. 2402080.
136. Milivojević, M.; Orozović, M.; Picozzi, S.; Gmitra, M.; Stavrić, S. Interplay of altermagnetism and weak ferromagnetism in two-dimensional RuF<sub>4</sub>. *2D Materials* **2024**, *11*, 035025.
137. Dmitrienko, V.; Ovchinnikova, E.; Collins, S.; Nisbet, G.; Beutier, G.; Kvashnin, Y.; Mazurenko, V.; Lichtenstein, A.; Katsnelson, M. Measuring the Dzyaloshinskii–Moriya interaction in a weak ferromagnet. *Nature Physics* **2014**, *10*, 202–206.

138. He, R.; Wang, D.; Luo, N.; Zeng, J.; Chen, K.Q.; Tang, L.M. Nonrelativistic spin-momentum coupling in antiferromagnetic twisted bilayers. *Physical Review Letters* **2023**, *130*, 046401.
139. Liu, Y.; Yu, J.; Liu, C.C. Twisted magnetic van der Waals bilayers: an ideal platform for altermagnetism. *Physical Review Letters* **2024**, *133*, 206702.
140. Miao, N.; Xu, B.; Zhu, L.; Zhou, J.; Sun, Z. 2D intrinsic ferromagnets from van der Waals antiferromagnets. *Journal of the American Chemical Society* **2018**, *140*, 2417–2420.
141. Feng, Y.; Peng, R.; Dai, Y.; Huang, B.; Duan, L.; Ma, Y. Antiferromagnetic ferroelastic multiferroics in single-layer VOX (X= Cl, Br) predicted from first-principles. *Applied Physics Letters* **2021**, *119*.
142. Shen, Z.X.; Su, C.; He, L. High-throughput computation and structure prototype analysis for two-dimensional ferromagnetic materials. *npj Computational Materials* **2022**, *8*, 132.
143. Zhang, S.; Xu, R.; Luo, N.; Zou, X. Two-dimensional magnetic materials: structures, properties and external controls. *Nanoscale* **2021**, *13*, 1398–1424.
144. Torelli, D.; Moustafa, H.; Jacobsen, K.W.; Olsen, T. High-throughput computational screening for two-dimensional magnetic materials based on experimental databases of three-dimensional compounds. *npj Computational Materials* **2020**, *6*, 158.
145. Khan, I.; Bezzerger, D.; Marfoua, B.; Hong, J. Altermagnetism, piezovoltage, and ferroelectricity in two-dimensional Cr<sub>2</sub>SeO altermagnet. *npj 2D Materials and Applications* **2025**, *9*, 18.
146. Guo, S.D.; Guo, X.S.; Cheng, K.; Wang, K.; Ang, Y.S. Piezoelectric altermagnetism and spin-valley polarization in Janus monolayer Cr<sub>2</sub>SO. *Applied Physics Letters* **2023**, *123*.
147. Yan, X.; Su, X.; Chen, J.; Jin, C.; Chen, L. Two-Dimensional Metal-Organic Frameworks Towards Spintronics. *Angewandte Chemie* **2023**, *135*, e202305408.
148. Che, Y.; Lv, H.; Wu, X.; Yang, J. Realizing altermagnetism in two-dimensional metal–organic framework semiconductors with electric-field-controlled anisotropic spin current. *Chemical Science* **2024**, *15*, 13853–13863.
149. López-Cabrelles, J.; Mañas-Valero, S.; Vitorica-Yrezabal, I.J.; Šiškins, M.; Lee, M.; Steeneken, P.G.; Van Der Zant, H.S.; Minguez Espallargas, G.; Coronado, E. Chemical design and magnetic ordering in thin layers of 2D metal–organic frameworks (MOFs). *Journal of the American Chemical Society* **2021**, *143*, 18502–18510.
150. Chakraborty, A.; González Hernández, R.; Šmejkal, L.; Sinova, J. Strain-induced phase transition from antiferromagnet to altermagnet. *Physical Review B* **2024**, *109*, 144421.
151. Fan, Z.; Zhang, Z.; Wang, H.; Gong, J.; Wang, D.; Wang, B. High-pressure modulation of altermagnetism in MnF<sub>2</sub>. *Applied Physics Letters* **2025**, *126*.
152. Leeb, V.; Mook, A.; Šmejkal, L.; Knolle, J. Spontaneous Formation of Altermagnetism from Orbital Ordering. *Physical Review Letters* **2024**, *132*, 236701.
153. Kim, H.; Yoshida, Y.; Lee, C.C.; Chang, T.R.; Jeng, H.T.; Lin, H.; Haga, Y.; Fisk, Z.; Hasegawa, Y. Atomic-scale visualization of surface-assisted orbital order. *Science advances* **2017**, *3*, eaao0362.
154. Murakami, Y.; Hill, J.; Gibbs, D.; Blume, M.; Koyama, I.; Tanaka, M.; Kawata, H.; Arima, T.; Tokura, Y.; Hirota, K.; et al. Resonant x-ray scattering from orbital ordering in LaMnO<sub>3</sub>. *Physical review letters* **1998**, *81*, 582.
155. Murakami, Y.; Kawada, H.; Kawata, H.; Tanaka, M.; Arima, T.; Moritomo, Y.; Tokura, Y. Direct observation of charge and orbital ordering in La<sub>0.5</sub>Sr<sub>1.5</sub>MnO<sub>4</sub>. *Physical review letters* **1998**, *80*, 1932.
156. Mizokawa, T.; Khomskii, D.; Sawatzky, G. Interplay between orbital ordering and lattice distortions in LaMnO<sub>3</sub>, YVO<sub>3</sub>, and YTiO<sub>3</sub>. *Physical Review B* **1999**, *60*, 7309.
157. Khaliullin, G.; Horsch, P.; Oleś, A.M. Spin order due to orbital fluctuations: Cubic vanadates. *Physical review letters* **2001**, *86*, 3879.
158. Jaeschke-Ubiergo, R.; Bharadwaj, V.K.; Jungwirth, T.; Šmejkal, L.; Sinova, J. Supercell altermagnets. *Physical Review B* **2024**, *109*, 094425.
159. Zhang, L.; Mei, L.; Wang, K.; Lv, Y.; Zhang, S.; Lian, Y.; Liu, X.; Ma, Z.; Xiao, G.; Liu, Q.; et al. Advances in the application of perovskite materials. *Nano-Micro Letters* **2023**, *15*, 177.
160. Kumar, N.S.; Naidu, K.C.B. A review on perovskite solar cells (PSCs), materials and applications. *Journal of Materiomics* **2021**, *7*, 940–956.
161. Bati, A.S.; Zhong, Y.L.; Burn, P.L.; Nazeeruddin, M.K.; Shaw, P.E.; Batmunkh, M. Next-generation applications for integrated perovskite solar cells. *Communications Materials* **2023**, *4*, 2.
162. Sanga, L.; Lalengmawia, C.; Renthlei, Z.; Chanu, S.T.; Hima, L.; Singh, N.S.; Yvaz, A.; Bhattarai, S.; Rai, D. A review on perovskite materials for photovoltaic applications. *Next Materials* **2025**, *7*, 100494.
163. Naka, M.; Motome, Y.; Seo, H. Altermagnetic perovskites. *npj Spintronics* **2025**, *3*, 1.
164. Naka, M.; Motome, Y.; Seo, H. Anomalous Hall effect in antiferromagnetic perovskites. *Physical Review B* **2022**, *106*, 195149.

165. Bernardini, F.; Fiebig, M.; Cano, A. Ruddlesden-Popper and perovskite phases as a material platform for altermagnetism. *arXiv preprint arXiv:2401.12910* **2024**.
166. Komarek, A.; Streltsov, S.; Isobe, M.; Möller, T.; Hoelzel, M.; Senyshyn, A.; Trots, D.; Fernández-Díaz, M.; Hansen, T.; Gotou, H.; et al. CaCrO<sub>3</sub>: an anomalous antiferromagnetic metallic oxide. *Physical Review Letters* **2008**, *101*, 167204.
167. Bordet, P.; Chaillout, C.; Marezio, M.; Huang, Q.; Santoro, A.; Cheong, S.; Takagi, H.; Oglesby, C.; Batlogg, B. Structural aspects of the crystallographic-magnetic transition in LaVO<sub>3</sub> around 140 K. *Journal of Solid State Chemistry* **1993**, *106*, 253–270.
168. Miyasaka, S.; Okimoto, Y.; Iwama, M.; Tokura, Y. Spin-orbital phase diagram of perovskite-type RVO<sub>3</sub> (R= rare-earth ion or Y). *Physical Review B* **2003**, *68*, 100406.
169. Miyasaka, S.; Okuda, T.; Tokura, Y. Critical behavior of metal-insulator transition in La<sub>1-x</sub>Sr<sub>x</sub>VO<sub>3</sub>. *Physical Review Letters* **2000**, *85*, 5388.
170. Solovyev, I. Magneto-optical effect in the weak ferromagnets LaMO<sub>3</sub> (M= Cr, Mn, and Fe). *Physical Review B* **1997**, *55*, 8060.
171. Kajimoto, R.; Yoshizawa, H.; Tomioka, Y.; Tokura, Y. Stripe-type charge ordering in the metallic A-type antiferromagnet Pr<sub>0.5</sub>Sr<sub>0.5</sub>MnO<sub>3</sub>. *Physical Review B* **2002**, *66*, 180402.
172. Okugawa, T.; Ohno, K.; Noda, Y.; Nakamura, S. Weakly spin-dependent band structures of antiferromagnetic perovskite LaMO<sub>3</sub> (M= Cr, Mn, Fe). *Journal of Physics: Condensed Matter* **2018**, *30*, 075502.
173. Zhou, J.S.; Alonso, J.; Muon, A.; Fernández-Díaz, M.; Goodenough, J. Magnetic structure of LaCrO<sub>3</sub> perovskite under high pressure from in situ neutron diffraction. *Physical Review Letters* **2011**, *106*, 057201.
174. Jüdin, V.; Sherman, A. Weak ferromagnetism of YCrO<sub>3</sub>. *Solid State Communications* **1966**, *4*, 661–663.
175. Tiwari, B.; Surendra, M.K.; Rao, M.R. HoCrO<sub>3</sub> and YCrO<sub>3</sub>: a comparative study. *Journal of Physics: Condensed Matter* **2013**, *25*, 216004.
176. Skumryev, V.; Ott, F.; Coey, J.; Anane, A.; Renard, J.P.; Pinsard-Gaudart, L.; Revcolevschi, A. Weak ferromagnetism in LaMnO<sub>3</sub>. *The European Physical Journal B-Condensed Matter and Complex Systems* **1999**, *11*, 401–406.
177. Bousquet, E.; Cano, A. Non-collinear magnetism in multiferroic perovskites. *Journal of Physics: Condensed Matter* **2016**, *28*, 123001.
178. White, R. Review of recent work on the magnetic and spectroscopic properties of the rare-earth orthoferrites. *Journal of Applied Physics* **1969**, *40*, 1061–1069.
179. Dixon, C.A.; Kavanagh, C.M.; Knight, K.S.; Kockelmann, W.; Morrison, F.D.; Lightfoot, P. Thermal evolution of the crystal structure of the orthorhombic perovskite LaFeO<sub>3</sub>. *Journal of Solid State Chemistry* **2015**, *230*, 337–342.
180. Bharadwaj, P.; Kollipara, V.S. Evaluating the structure-property correlation in Y<sub>1-x</sub>Nd<sub>x</sub>FeO<sub>3</sub> (0 ≤ x ≤ 0.15) perovskites. *Ceramics International* **2021**, *47*, 30797–30806.
181. Shane, J.; Lyons, D.; Kestigian, M. Antiferromagnetic resonance in NaMnF<sub>3</sub>. *Journal of Applied Physics* **1967**, *38*, 1280–1282.
182. Beckman, O.; Knox, K. Magnetic Properties of KMnF<sub>3</sub>. I. Crystallographic Studies. *Physical Review* **1961**, *121*, 376.
183. Heeger, A.; Beckman, O.; Portis, A. Magnetic Properties of KMnF<sub>3</sub>. II. Weak Ferromagnetism. *Physical Review* **1961**, *123*, 1652.
184. Sattigeri, R.M.; Cuono, G.; Autieri, C. Altermagnetic surface states: towards the observation and utilization of altermagnetism in thin films, interfaces and topological materials. *Nanoscale* **2023**, *15*, 16998–17005.
185. Feng, Z.; Zhou, X.; Šmejkal, L.; Wu, L.; Zhu, Z.; Guo, H.; González-Hernández, R.; Wang, X.; Yan, H.; Qin, P.; et al. An anomalous Hall effect in altermagnetic ruthenium dioxide. *Nature Electronics* **2022**, *5*, 735–743.
186. Zhou, X.; Feng, W.; Zhang, R.W.; Šmejkal, L.; Sinova, J.; Mokrousov, Y.; Yao, Y. Crystal thermal transport in altermagnetic RuO<sub>2</sub>. *Physical review letters* **2024**, *132*, 056701.
187. Mazin, I.I. Notes on altermagnetism and superconductivity. *arXiv preprint arXiv:2203.05000* **2022**.
188. Nagaosa, N.; Sinova, J.; Onoda, S.; MacDonald, A.H.; Ong, N.P. Anomalous hall effect. *Reviews of modern physics* **2010**, *82*, 1539–1592.
189. Chen, H.; Niu, Q.; MacDonald, A.H. Anomalous Hall effect arising from noncollinear antiferromagnetism. *Physical review letters* **2014**, *112*, 017205.
190. Kübler, J.; Felser, C. Non-collinear antiferromagnets and the anomalous Hall effect. *Europhysics Letters* **2014**, *108*, 67001.



191. Nakatsuji, S.; Kiyohara, N.; Higo, T. Large anomalous Hall effect in a non-collinear antiferromagnet at room temperature. *Nature* **2015**, *527*, 212–215.
192. Sürgers, C.; Kittler, W.; Wolf, T.; Löhneysen, H.v. Anomalous Hall effect in the noncollinear antiferromagnet Mn<sub>5</sub>Si<sub>3</sub>. *AIP Advances* **2016**, *6*.
193. Boldrin, D.; Samathrakris, I.; Zemen, J.; Mihai, A.; Zou, B.; Johnson, F.; Esser, B.D.; McComb, D.W.; Petrov, P.K.; Zhang, H.; et al. Anomalous Hall effect in noncollinear antiferromagnetic Mn<sub>3</sub>NiN thin films. *Physical Review Materials* **2019**, *3*, 094409.
194. Šmejkal, L.; MacDonald, A.H.; Sinova, J.; Nakatsuji, S.; Jungwirth, T. Anomalous hall antiferromagnets. *Nature Reviews Materials* **2022**, *7*, 482–496.
195. Ghimire, N.J.; Botana, A.; Jiang, J.; Zhang, J.; Chen, Y.S.; Mitchell, J. Large anomalous Hall effect in the chiral-lattice antiferromagnet CoNb<sub>3</sub>S<sub>6</sub>. *Nature communications* **2018**, *9*, 3280.
196. Naka, M.; Hayami, S.; Kusunose, H.; Yanagi, Y.; Motome, Y.; Seo, H. Anomalous Hall effect in  $\kappa$ -type organic antiferromagnets. *Physical Review B* **2020**, *102*, 075112.
197. Attias, L.; Levchenko, A.; Khodas, M. Intrinsic anomalous Hall effect in altermagnets. *Physical Review B* **2024**, *110*, 094425.
198. Leiviskä, M.; Rial, J.; Bad'ura, A.; Seeger, R.L.; Kounta, I.; Beckert, S.; Kriegner, D.; Joumard, I.; Schmoranzarová, E.; Sinova, J.; et al. Anisotropy of the anomalous Hall effect in thin films of the altermagnet candidate Mn<sub>5</sub>Si<sub>3</sub>. *Physical Review B* **2024**, *109*, 224430.
199. Tschirner, T.; Keßler, P.; Gonzalez Betancourt, R.D.; Kotte, T.; Kriegner, D.; Büchner, B.; Dufouleur, J.; Kamp, M.; Jovic, V.; Smejkal, L.; et al. Saturation of the anomalous Hall effect at high magnetic fields in altermagnetic RuO<sub>2</sub>. *APL Materials* **2023**, *11*.
200. Jin, H.; Tan, Z.; Gong, Z.; Wang, J. Anomalous Hall effect in two-dimensional vanadium tetrahalogen with altermagnetic phase. *Physical Review B* **2024**, *110*, 155125.
201. Betancourt, R.G.; Zubáč, J.; Gonzalez-Hernandez, R.; Geishendorf, K.; Šobán, Z.; Springholz, G.; Olejník, K.; Šmejkal, L.; Sinova, J.; Jungwirth, T.; et al. Spontaneous anomalous Hall effect arising from an unconventional compensated magnetic phase in a semiconductor. *Physical Review Letters* **2023**, *130*, 036702.
202. Nguyen, T.P.T.; Yamauchi, K. Ab initio prediction of anomalous Hall effect in antiferromagnetic CaCrO<sub>3</sub>. *Physical Review B* **2023**, *107*, 155126.
203. Hou, X.Y.; Yang, H.C.; Liu, Z.X.; Guo, P.J.; Lu, Z.Y. Large intrinsic anomalous Hall effect in both Nb<sub>2</sub>FeB<sub>2</sub> and Ta<sub>2</sub>FeB<sub>2</sub> with collinear antiferromagnetism. *Physical Review B* **2023**, *107*, L161109.
204. Wang, M.; Tanaka, K.; Sakai, S.; Wang, Z.; Deng, K.; Lyu, Y.; Li, C.; Tian, D.; Shen, S.; Ogawa, N.; et al. Emergent zero-field anomalous Hall effect in a reconstructed rutile antiferromagnetic metal. *Nature Communications* **2023**, *14*, 8240.
205. Reichlová, H.; Seeger, R.L.; González-Hernández, R.; Kounta, I.; Schlitz, R.; Kriegner, D.; Ritzinger, P.; Lammel, M.; Leiviskä, M.; Petříček, V.; et al. Macroscopic time reversal symmetry breaking arising from antiferromagnetic Zeeman effect **2024**.
206. Kluczyk, K.; Gas, K.; Grzybowski, M.; Skupiński, P.; Borysiewicz, M.; Fas, T.; Suffczyński, J.; Domagala, J.; Grasa, K.; Mycielski, A.; et al. Coexistence of anomalous Hall effect and weak magnetization in a nominally collinear antiferromagnet MnTe. *Physical Review B* **2024**, *110*, 155201.
207. Šmejkal, L.; Mokrousov, Y.; Yan, B.; MacDonald, A.H. Topological antiferromagnetic spintronics. *Nature physics* **2018**, *14*, 242–251.
208. Hasan, M.Z.; Chang, G.; Belopolski, I.; Bian, G.; Xu, S.Y.; Yin, J.X. Weyl, Dirac and high-fold chiral fermions in topological quantum matter. *Nature Reviews Materials* **2021**, *6*, 784–803.
209. Bradlyn, B.; Cano, J.; Wang, Z.; Vergniory, M.; Felser, C.; Cava, R.J.; Bernevig, B.A. Beyond Dirac and Weyl fermions: Unconventional quasiparticles in conventional crystals. *Science* **2016**, *353*, aaf5037.
210. Thomson, W. XIX. On the electro-dynamic qualities of metals:—Effects of magnetization on the electric conductivity of nickel and of iron. *Proceedings of the Royal Society of London* **1857**, pp. 546–550.
211. Baibich, M.N.; Broto, J.M.; Fert, A.; Van Dau, F.N.; Petroff, F.; Etienne, P.; Creuzet, G.; Friederich, A.; Chazelas, J. Giant magnetoresistance of (001) Fe/(001) Cr magnetic superlattices. *Physical review letters* **1988**, *61*, 2472.
212. Binasch, G.; Grünberg, P.; Saurenbach, F.; Zinn, W. Enhanced magnetoresistance in layered magnetic structures with antiferromagnetic interlayer exchange. *Physical review B* **1989**, *39*, 4828.
213. Miyazaki, T.; Tezuka, N. Giant magnetic tunneling effect in Fe/Al<sub>2</sub>O<sub>3</sub>/Fe junction. *Journal of magnetism and magnetic materials* **1995**, *139*, L231–L234.
214. Moodera, J.S.; Kinder, L.R.; Wong, T.M.; Meservey, R. Large magnetoresistance at room temperature in ferromagnetic thin film tunnel junctions. *Physical review letters* **1995**, *74*, 3273.



215. Slonczewski, J.C. Current-driven excitation of magnetic multilayers. *Journal of Magnetism and Magnetic Materials* **1996**, *159*, L1–L7.
216. Berger, L. Emission of spin waves by a magnetic multilayer traversed by a current. *Physical Review B* **1996**, *54*, 9353.
217. Jabeur, K.; Buda-Prejbeanu, L.; Prenat, G.; Di Pendina, G. Study of two writing schemes for a magnetic tunnel junction based on spin orbit torque. In Proceedings of the Proceedings of World Academy of Science, Engineering and Technology. World Academy of Science, Engineering and Technology (WASET), 2013, number 80, p. 517.
218. Nguyen, V.; Rao, S.; Wostyn, K.; Couet, S. Recent progress in spin-orbit torque magnetic random-access memory. *npj Spintronics* **2024**, *2*, 48.
219. Chappert, C.; Fert, A.; Van Dau, F.N. The emergence of spin electronics in data storage. *Nature materials* **2007**, *6*, 813–823.
220. Bhatti, S.; Sbiaa, R.; Hirohata, A.; Ohno, H.; Fukami, S.; Piramanayagam, S. Spintronics based random access memory: a review. *Materials today* **2017**, *20*, 530–548.
221. Bader, S.D.; Parkin, S.S.P. Spintronics. *Annu. Rev. Condens. Matter Phys.* **2010**, *1*, 71–88.
222. Manchon, A.; Železný, J.; Miron, I.M.; Jungwirth, T.; Sinova, J.; Thiaville, A.; Garello, K.; Gambardella, P. Current-induced spin-orbit torques in ferromagnetic and antiferromagnetic systems. *Reviews of Modern Physics* **2019**, *91*, 035004.
223. Železný, J.; Gao, H.; Vyborný, K.; Zemen, J.; Mašek, J.; Manchon, A.; Wunderlich, J.; Sinova, J.; Jungwirth, T. Relativistic Néel-order fields induced by electrical current in antiferromagnets. *Physical review letters* **2014**, *113*, 157201.
224. Wadley, P.; Howells, B.; Železný, J.; Andrews, C.; Hills, V.; Campion, R.P.; Novák, V.; Olejník, K.; Maccherozzi, F.; Dhesi, S.; et al. Electrical switching of an antiferromagnet. *Science* **2016**, *351*, 587–590.
225. Wadley, P.; Reimers, S.; Grzybowski, M.J.; Andrews, C.; Wang, M.; Chauhan, J.S.; Gallagher, B.L.; Campion, R.P.; Edmonds, K.W.; Dhesi, S.S.; et al. Current polarity-dependent manipulation of antiferromagnetic domains. *Nature nanotechnology* **2018**, *13*, 362–365.
226. Zhang, Y.; Xu, Q.; Koepernik, K.; Rezaev, R.; Janson, O.; Železný, J.; Jungwirth, T.; Felser, C.; van den Brink, J.; Sun, Y. Different types of spin currents in the comprehensive materials database of nonmagnetic spin Hall effect. *npj Computational Materials* **2021**, *7*, 167.
227. Tanaka, K.; Nomoto, T.; Arita, R. First-principles study of the tunnel magnetoresistance effect with Cr-doped RuO<sub>2</sub> electrode. *Physical Review B* **2024**, *110*, 064433.
228. Qin, P.; Yan, H.; Wang, X.; Chen, H.; Meng, Z.; Dong, J.; Zhu, M.; Cai, J.; Feng, Z.; Zhou, X.; et al. Room-temperature magnetoresistance in an all-antiferromagnetic tunnel junction. *Nature* **2023**, *613*, 485–489.
229. Duine, R.; Lee, K.J.; Parkin, S.S.; Stiles, M.D. Synthetic antiferromagnetic spintronics. *Nature physics* **2018**, *14*, 217–219.
230. Schlauderer, S.; Lange, C.; Baierl, S.; Ebnet, T.; Schmid, C.P.; Valovcin, D.; Zvezdin, A.; Kimel, A.; Mikhaylovskiy, R.; Huber, R. Temporal and spectral fingerprints of ultrafast all-coherent spin switching. *Nature* **2019**, *569*, 383–387.
231. Landauer, R. Irreversibility and heat generation in the computing process. *IBM journal of research and development* **1961**, *5*, 183–191.
232. Bennett, C.H. The thermodynamics of computation—a review. *International Journal of Theoretical Physics* **1982**, *21*, 905–940.
233. Hong, J.; Lambson, B.; Dhuey, S.; Bokor, J. Experimental test of Landauer’s principle in single-bit operations on nanomagnetic memory bits. *Science advances* **2016**, *2*, e1501492.
234. Gaudenzi, R.; Burzurí, E.; Maegawa, S.; Van Der Zant, H.; Luis, F. Quantum Landauer erasure with a molecular nanomagnet. *Nature Physics* **2018**, *14*, 565–568.
235. Kimel, A.; Kalashnikova, A.; Pogrebna, A.; Zvezdin, A. Fundamentals and perspectives of ultrafast photoferroic recording. *Physics Reports* **2020**, *852*, 1–46.
236. Han, L.; Fu, X.; He, W.; Zhu, Y.; Dai, J.; Yang, W.; Zhu, W.; Bai, H.; Chen, C.; Wan, C.; et al. Observation of non-volatile anomalous Nernst effect in altermagnet with collinear Néel vector. *arXiv preprint arXiv:2403.13427* **2024**.
237. Yang, Y.; Li, J.; Yin, J.; Xu, S.; Mullan, C.; Taniguchi, T.; Watanabe, K.; Geim, A.K.; Novoselov, K.S.; Mishchenko, A. In situ manipulation of van der Waals heterostructures for twistrionics. *Science advances* **2020**, *6*, eabd3655.

238. Tang, B.; Che, B.; Xu, M.; Ang, Z.P.; Di, J.; Gao, H.J.; Yang, H.; Zhou, J.; Liu, Z. Recent advances in synthesis and study of 2D twisted transition metal dichalcogenide bilayers. *Small Structures* **2021**, *2*, 2000153.
239. Poretzky, A.A.; Liang, L.; Li, X.; Xiao, K.; Sumpter, B.G.; Meunier, V.; Geohegan, D.B. Twisted MoSe<sub>2</sub> bilayers with variable local stacking and interlayer coupling revealed by low-frequency Raman spectroscopy. *ACS nano* **2016**, *10*, 2736–2744.
240. Huang, S.; Ling, X.; Liang, L.; Kong, J.; Terrones, H.; Meunier, V.; Dresselhaus, M.S. Probing the interlayer coupling of twisted bilayer MoS<sub>2</sub> using photoluminescence spectroscopy. *Nano letters* **2014**, *14*, 5500–5508.
241. Chen, X.D.; Xin, W.; Jiang, W.S.; Liu, Z.B.; Chen, Y.; Tian, J.G. High-precision twist-controlled bilayer and trilayer graphene. *Advanced Materials* **2016**, *28*, 2563–2570.
242. Wang, K.; Huang, B.; Tian, M.; Ceballos, F.; Lin, M.W.; Mahjouri-Samani, M.; Boulesbaa, A.; Poretzky, A.A.; Rouleau, C.M.; Yoon, M.; et al. Interlayer coupling in twisted WSe<sub>2</sub>/WS<sub>2</sub> bilayer heterostructures revealed by optical spectroscopy. *ACS nano* **2016**, *10*, 6612–6622.
243. Sun, X.; Suriyage, M.; Khan, A.R.; Gao, M.; Zhao, J.; Liu, B.; Hasan, M.M.; Rahman, S.; Chen, R.s.; Lam, P.K.; et al. Twisted van der Waals quantum materials: fundamentals, tunability, and applications. *Chemical Reviews* **2024**, *124*, 1992–2079.
244. Yao, W.; Wang, E.; Bao, C.; Zhang, Y.; Zhang, K.; Bao, K.; Chan, C.K.; Chen, C.; Avila, J.; Asensio, M.C.; et al. Quasicrystalline 30° twisted bilayer graphene as an incommensurate superlattice with strong interlayer coupling. *Proceedings of the National Academy of Sciences* **2018**, *115*, 6928–6933.
245. Lim, C.y.; Kim, S.; Jung, S.W.; Hwang, J.; Kim, Y. Recent technical advancements in ARPES: Unveiling quantum materials. *Current Applied Physics* **2024**, *60*, 43–56.
246. Samanta, K.; Ležaić, M.; Merte, M.; Freimuth, F.; Blügel, S.; Mokrousov, Y. Crystal Hall and crystal magneto-optical effect in thin films of SrRuO<sub>3</sub>. *Journal of applied physics* **2020**, *127*.
247. Zhou, X.; Feng, W.; Yang, X.; Guo, G.Y.; Yao, Y. Crystal chirality magneto-optical effects in collinear antiferromagnets. *Physical Review B* **2021**, *104*, 024401.
248. Iguchi, S.; Kobayashi, H.; Ikemoto, Y.; Furukawa, T.; Itoh, H.; Iwai, S.; Moriwaki, T.; Sasaki, T. Magneto-optical detection of altermagnetism in organic antiferromagnet. *arXiv preprint arXiv:2409.15696* **2024**.
249. Flebus, B.; Grundler, D.; Rana, B.; Otani, Y.; Barsukov, I.; Barman, A.; Gubbiotti, G.; Landeros, P.; Akerman, J.; Ebels, U.; et al. The 2024 magnonics roadmap. *Journal of Physics: Condensed Matter* **2024**, *36*, 363501.

**Disclaimer/Publisher's Note:** The statements, opinions and data contained in all publications are solely those of the individual author(s) and contributor(s) and not of MDPI and/or the editor(s). MDPI and/or the editor(s) disclaim responsibility for any injury to people or property resulting from any ideas, methods, instructions or products referred to in the content.